UNIVERSITÀ DEGLI STUDI DI PALERMO
Dottorato in "Tecnologie e Scienze per la Salute dell'Uomo"
Dipartimento Biomedico di Medicina Interna e Specialistica DIBIMIS
Settore Scientifico Disciplinare BIO/10

DEVELOPMENT AND QUALIFICATION OF BIOANALYTICAL METHODS FOR DEAMIDATED IFNβ-1a AND INVESTIGATION ABOUT THE MECHANISM OF ACTION

IL DOTTORE
Elisa Lipari

IL COORDINATORE
Prof. Maurizio Leone

ILTUTOR
Prof. Giulio Ghersi

TUTOR AZIENDALE
Dott. Cosimo-Walter D'Acunto
Merck Serono Spa

CICLO XXXIII
ANNO CONSEGUIMENTO TITOLO 2020/21

Development and qualification of bioanalytical methods for deamidated IFNβ-1a and investigation about the mechanism of action.

Merck Serono S.p.A, Rome, Italy; an affiliate of Merck KGaA, Darmstadt, Germany.

Abstract

Interferon beta-1a (IFNβ-1a) is a recombinant IFNβ with the tradename Rebif involved in several biological activities. Recently, it has been reported that artificial deamidation of IFNb-1a increases its biological response. Given the therapeutical potential, an investigation on the deamidated variant has been carried out via different approaches to discover the mechanism underlying this biological effect. The antiviral and immunomodulatory activity of deamidated cytokine was assessed using two precise and accurate cell-based assays. As expected, deamidated IFNβ-1a showed an increase in the biological response and its canonical pathway and receptor binding affinity were thorough analysed. Deamidated interferon beta increases STAT1 phosphorylation and ISGs expression compared to its native form. A full in-depth analysis in receptor binding highlighted a change in receptor affinity in deamidated IFNβ-1a. In particular, deamidation destabilizes the interaction with IFNAR2 through a change in the H-bonds network, increasing the affinity to IFNAR1 and consequently to the whole receptor complex. The higher receptor binding and the consequent strong signaling and gene expression, explains the greater biological activity of the deamidated IFNβ-1a compared to the native fcorm. These results open new perspective on the therapeutic potential of this molecule which could have significant beneficial effects on patients with MS and beyond.

Table of Contents

1 INTRODUCTION

1.1 INTERFERONS ORIGINS AND CLASSIFICATION

Type I interferons are widely expressed cytokines characterized by several biological functions, mainly antiviral, antiproliferative and immunomodulatory activities.

Interferon interest starts after 1957 when a family of cytokines capable of interfering with viral replication was discovered in jawed vertebrates and its members were called "interferons"[1]. In a short time, interferons were found to be produced in many animals, tissues and cells and they attracted worldwide attention [2]. It was nearly two decades after the initial description of Interferons that methods were developed to allow sufficient purification and more rigorous characterization of IFN's properties[3]. In 1978, an interferon was purified for the first time so that it could be analyzed and characterized. As purification schemes were being refined, it became apparent that IFN was not one, but a family of distinct proteins.

Over the years, about 10 mammalian interferon species have been discovered, but only seven are found in humans. Previously, interferons were classified based on their cell origin. However, other cell types have shown to produced IFNs too. For this reason, the previous designation has been replaced by a more precise classification based on molecular characterization after the isolation, cloning and sequencing of the IFNs multigene family. They were resorted into interferon types I,II, and III in accordance with their receptors [2,4]. Type I interferon, which comprises α andβ interferons can be further divided into different subtypes based on their different antigenicity. These subtypes are indicated by Greek letters and can be further sorted into even smaller categories (Figure 1).

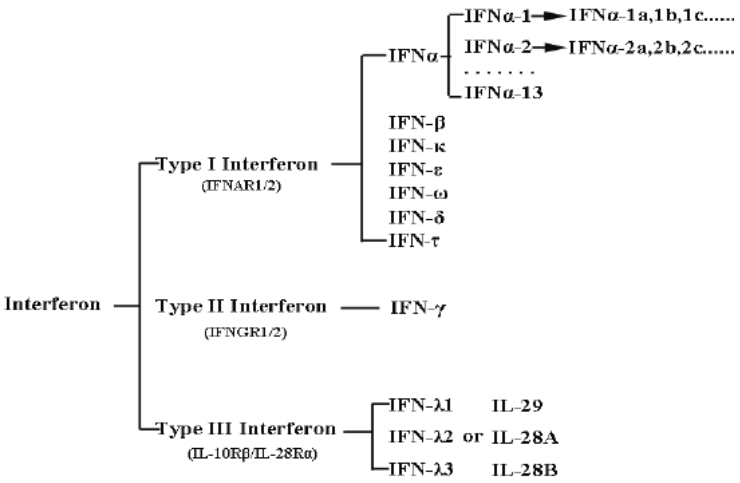

Figure 1: IFNs classification. Interferons have been classified into three major types based on the receptor through which they signal. Except Type II interferon, each of them contains subtypes. From "Overview of interferon: characteristic, signaling and anti-cancer effect" [2].

Initially, researchers only knew IFNs existence and function, but they were unable to obtain enough amounts of this cytokine for further research and clinical applications. Much larger quantities of IFN could be made available 29 years after its discovery and a high-quality interferon production increases remarkably with the development of genetic engineering. This allowed for its widespread application in both research and clinical settings, which ushered in a new era for interferons[5].

1.2 INTERFERON BETA AND ITS RECEPTOR STRUCTURE

Focusing on Human IFNβ (hu-IFNβ), it is a 166-aminoacid glycoprotein with a molecular weight of 22.5 KDa. It is characterized by a 35% sequence identity to the consensus sequence of IFNα and 50% sequence identity to murine IFNβ (mu-IFNβ).

Structurally, IFNβ is dominated by five α-helix, along with short stretches of 310 helix in adjoining sequences and connecting loops. According to Presnell and Cohen[6], IFNβ may be classified as a left-handed, type 2 helix bundle defined by helices *A*, *B*,*C* and *E*. Helix *A* runs parallel with helix *B* and antiparallel with helices *C* and *E*; helix *D* is part of the long loop connecting helices *C* and *E*. Moreover, there are two additional remarkable elements in the covalent structure of hu-IFNβ: a disulphide bridge between Cys31 of loop *A*-*B* and Cys141 of loop *D*-*E* (Figure 2*)*. Both loops play an important role in receptor interactions and the disulphide linkage may act to coordinate their structure[7].

Additionally, unlike IFNα, Hu-IFNβ is N-glycosylated at a single site in Asn 80 at the end of helix *C*[8] (Figure 2).

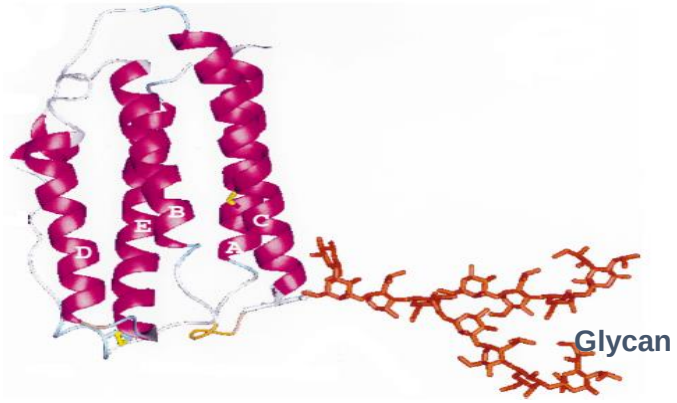

Figure 2: in silico structure of Hu-IFNβ. In magenta, the A-E helix. In yellow, the cysteine and in orange the glycan are represented. From "The structure of human interferon-b: implications for activity"[7].

Type I IFNs exert their biological effect through the binding to the common IFNα/β receptor, named IFNAR.

This heterodimeric receptor includes the high affinity subunit IFNAR2 and the low affinity subunit IFNAR1[9].

IFNs receptors were identified 10 years later the IFNs discovery and different variant isoform of both receptor subunit that contribute to the potential complexity of the functional receptor were identified.

IFNAR1 and IFNAR2 belong to the class II helical Cytokine Receptor (hCR) family. Like other receptors in this class, the ectodomain (ECD) of the high-affinity subunit IFNAR2 comprises two fibronectin type III (FNIII)-like subdomains referred to as D1 and D2, respectively.

huIFNAR1 ECD contains four FNIII-like subdomains, called as SD1–SD4 which most likely emerged from gene duplication.SD1–SD3 subdomain appear to house the ligand binding domain while SD4 is essential for ternary complex formation. The SD1-SD2 pair is structurally similar to the SD3-SD4 pair with characteristic disulfide-bonding cysteine pairs and 50% sequence homology (Figure 3) [10,11].

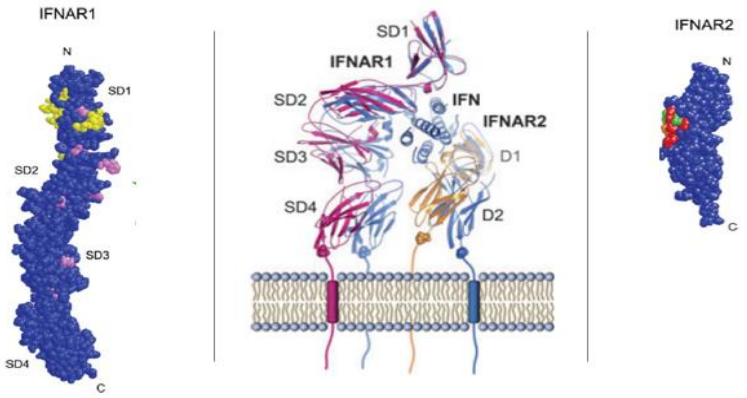

Figure 3: The type I IFN receptor. On the left, Amino acid residues of IFNAR1 ECD that reportedly interact with membrane-bound glycosphingolipids are shown in yellow. Amino acid important for huIFNs binding are colored in violet. On the right, the huIFNAR2 ECD structure shows amino acid residues that are important for the binding of HuIFNα (red) or HuIFNβ (green) and the residues important for binding both ligands (orange).In the middle, in silico structure of ternary complex and IFNAR domains. Images from: J. Piehler et al. [11]

IFNs interact differently with the extracellular portions of IFNAR1 and IFNAR2, thus giving rise to distinct activated states of the receptor. IFNβ bind first to the high-affinity IFNAR2 chain and the resulting IFN:IFNAR2 complex subsequently recruits IFNAR1 to form the ternary, activated complex (Figure 4)[12].

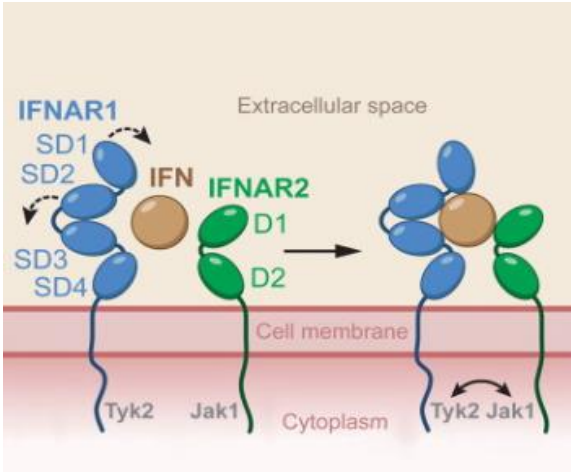

Figure 4: IFNβ-IFNAR binding and conformational changes. Receptor binding is a sequential process with the IFNs first binding to the higher affinity IFNAR2, followed by the recruitment of IFNAR1 to form the ternary complex with subsequent receptor activation. Moreover, the IFNs binding to its receptor induce a conformational change in IFNAR1 during ternary complex formation. Picture from: C. Thomas et al.[11]

Structural conformational change of receptor components upon ligand binding has an important role to propagate the signal to the cytoplasmic domains of the receptor chains.

In this process, the role of SD4-IFNAR1 domain has been well established. Conformational movement in SD4 suggests a transfer of signal from the IFN-binding site to the membrane-proximal domain of IFNAR1. Without this domain, IFNAR is unable to form a ternary complex and activate an IFN response[7,11].

All these binding characteristics allowed addressing the question how the binding affinity influences the IFNs biological activity. Receptor-ligand affinity is critical for regulating the signal strength through the membrane and the subsequent intracellular signaling (Deshpande et al, 2013). A correlation between receptor numbers, STAT activation and gene induction was observed.

Literature data suggest that the antiviral activity require very low ligand and receptor concentration and it is activated after a short ligand exposure. In contrast, the antiproliferative activity needs a high ligand and receptor concentration with a long IFN-IFNAR binding time [11]

Moreover,the number of receptor present in the cellular surface is a further factor that could affect the signaling pathway.

1.3 CANONICAL INTERFERON SIGNALING PATHWAY

Upon IFN binding to cell surface receptors, cytoplasmic signal transduction pathway is activated into the cell, leading to a number of 'IFN-inducible' genes expression. All IFNs act through the JAK-STAT canonical signaling pathway. In the absence of determined stimuli, the cytoplasmic domain of each IFNAR chain is bound by a specific JAK protein in an inactive conformation. Both heterodimeric receptors do not display any catalytic activity, instead, members of the receptor-associated Janus Kinases (JAK) family (JAK1, JAK2 and TYK2), which are constitutively associated with the heterodimeric receptors, get activated upon binding of IFNs. Thus, receptor chains are brought into close proximity, and the two receptor-associated protein tyrosine kinases Janus kinase 1 (JAK1) and tyrosine kinase 2 (TYK2) undergo transphosphorylation and sustained activation (Figure5)[13,14].

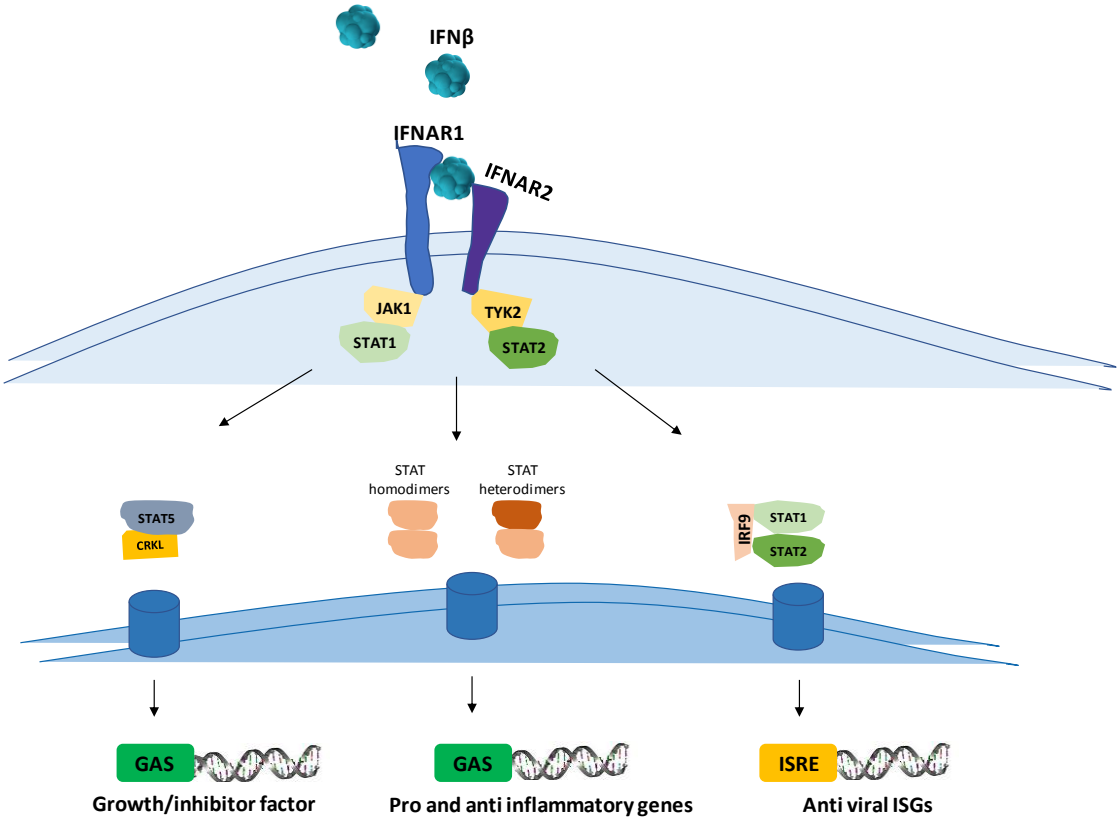

Figure 5: Canonical Type I IFNs signaling pathway. Upon binding of type I IFN to the IFNAR1/IFNAR2, transactivation of JAK1 and TYK2 leads to the phosphorylation of STATs proteins. After STATs phosphorylation three main complexes can be formed (STAT5/CrkL, STAT homo- or heterodimers, ISGF3 complex) and the related cellular responses are activated (growth inhibitory factors, pro- and anti-inflammatory response and antiviral response, respectively). Image created by Elisa Lipari.

Once activated, these kinases phosphorylate STAT proteins via Src homology 2 (SH2) domain interactions. As a result, STATs are phosphorylated on conserved tyrosine residues

and released from the receptor, where conformational changes lead to homo- or heterodimerization[11].

Three main complexes could be formed:

1) the ISGF3 complex (IRF9/p-STAT1/p-STAT2);

2) STAT5/CrkL;

3) STAT homo- or heterodimers.

All these complexes act as transcription factors driving the production of interferon stimulated genes through the binding of specific motifs in their promoter sequences: gamma-activated sequence (GAS) and IFN-stimulated response elements (ISRE) elements- The consequent different cellular response, mainly antiviral, antiproliferative and immunomodulatory, depends on the STATs complex activated [13].

Regarding the ISGF3 complex, tyrosine-phosphorylated STAT1 and STAT2 dimerize and bind the IFN-regulatory factor 9 (IRF9) to form a trimolecular complex called IFN-stimulated gene factor 3 (ISGF3). This transcription factor translocates to the nucleus and binds its cognate DNA sequences, ISREs within the promoter of IFN-stimulated genes (ISGs), to activated classical antiviral response [11,14].

In contrast, STAT5/CrkL complex translocate into the nucleus and bind GAS sequence to activate a growth inhibitory response. Finally, STAT hetero-homodimers bind GAS promoter activating inflammatory or anti-inflammatory response [13].

1.4 IFNs RELATED SIGNALING PATHWAY

In addition to the classical JAK-STAT pathway, the contribution of other signaling involved in IFNs activity, such as MAPK and NF-κB pathway, have been described by several scientific data. However, the actors of this signaling crosstalk are still unknown and seem to be related to cell type [15] [16].

The signaling pathway employing the mitogen activated ERK-activating kinase (MEK) and the extacellular-regulated kinase (ERK) are critical in growth factors signaling. Engagement of the receptor and subsequent stimulation of Ras and Raf, initiates a phosphorylating cascade leading to activation to several proteins among which MEK and ERK play a central role in controlling cell development, activation and proliferation.

In human hepatoma cells, Type I interferon up-regulates significantly ERK phosphorylation and led to a mild increase of the stressed-related signal transduction pathway pP38 and pJNK

after short-time treatment [15]. In contrast, MAPK activation was observed in transformed T- and monocytic cell lines only after a long-term exposure to IFNs treatment [16].

NF-kB pathway is also activated by type I interferon. The NF-kB transcription factor regulates the expression of genes involved in cell survival, cell growth, inflammation and immune response, which are all processes affected by IFNs. In the classical signaling pathway, NF-kB activity is tightly controlled by inhibitory IkB proteins, which bind to NF-kB complexes and sequester them in the cytoplasm. When stimulated by signals, usually coming from the outside of the cell, a kinase called the IkB Kinase (IKK) phosphorylates two serine residues leading to ubiquitination process and consequently degradation of IkB protein. With the degradation of IκB, the NF-κB complex is then free to enter the nucleus where it can regulate the expression of specific genes that have DNA-binding sites for NF-κB. The specific role of NF-κB is still unclear. In literature many authors report contrasting effects of NF-κB. Several results suggest that NF-κB pathway is essential to IFN-induced cell survival and there are multiple IFN-stimulated pathways leading to NF-κB activation. It was reported that within 30 min of IFN stimulation, NF-κB DNA-binding activity was induced in diverse cell types (lymphoblastoid, fibrosarcoma, renal carcinoma, and normal fibroblasts [17] [18]. In contrast, other literature data shows that interferon alpha inhibit NF-κB activity in a time- and dose-dependent manner and sensitizes cells to IFN's apoptotic and antiviral activities [19] [20].

1.4 MAIN IFNβCELLULAR RESPONSE

Once the signaling is initiated, different cellular response can be activated. Over the years several IFNβ functions have been discovered and it is now established that type I Interferon are a pleiotropic cytokine. They are widely used to treat chronic viral infections, mainly hepatitis B and C virus. Other interferon functions include growth inhibition of some tumors by inducing cell apoptosis, angiogenesis inhibition and cytotoxic activity against tumor cells. However, antiproliferative, antiviral and immunomodulatory, are the main biological activity reported.

- Antiviral activity: It is now seen as just one of many activities induced by IFNs and several proteins have been identified which play a role in suppressing viral

propagation. To complete their life cycle, viruses must enter cells, translate and replicate their genomes, and exit in order to infect new cells. In this scenario, type I IFNs induce the activation of 2-5A synthetase which catalyses the formation of an unusual oligonucleotide, ppp (A2Vp) nA (2-5A), required to activate a latent endonuclease, RNase L, which degrades viral mRNAs. Infected cells use this way to inhibit cytoplasmic replication of small RNA viruses such as murine encephalomyocarditis virus (EMCV) and Mengo virus. Further IFN-inducible proteins, for instance, the type I IFN-inducible Mx proteins, appear to specifically inhibit the replication of other groups of viruses, including influenza viruses [21]. Specifically, Mx proteins recognize the nucleoproteins or (nucleo)-capsid proteins of different viruses, perhaps concurrently with the viral polymerase.

- Antiproliferative Activity: It was first described in 1978, but the mechanism of its activation is still under discussion. It is well established that interferon is able to induce an antiproliferative state in many cells regulating the expression of different genes involved in the cell cycle and apoptosis. Several cell arrest mechanisms were described over the years, including suppression of cyclins resulting in G0/G1 arrest as well as transcriptional repression of the growth-promoting factor E2F-1. How IFNs initiate interferon-induced apoptosis is still unknown. The specific mechanism of cell cycle suppression depends on the cell type[2]. Moreover, the antiproliferative activity is not dependent from the antiviral activity. This last property required only 4 hours to induce a state of resistance against a viral attack in contrast to the antiproliferative IFNs ability that requires prolonged and continuous administration of high dose or tight-binding IFN for as long as 36 to 72 h before the effect is expressed[22]. The IFNβ antiproliferative activity was found also in specific tumor cells where IFNβ is able to suppress cell growth and leading to anti-cancer effects [2].

- Immunomodulatory activity: Interferon plays a key role also in inflammatory and immunosuppressive disease[1]. One of the immuno-mechanisms to clear viral infection by the host system, is the elimination of infected cells by cytotoxic T lymphocytes (CTL). This elimination mechanism requires CTL recognition of viral antigens presented on MHC class I of infected cells. In response to an infection, a cascade of signals activates inflammatory cells such as neutrophils and macrophages, which in turn produce cytokines and chemokines. If the inflammation is sustained and robust,

the overproduction of inflammatory cytokines can lead to other immune cells activation with consequent tissue damage and serious disorders. Interferons (IFNs) and inflammatory cytokines are crucial in this process and they may influence cellular, tissue, and global physiological functions[23].For its immunomodulatory activity, interferon-β has been found to be useful in the treatment of Multiple Sclerosis (MS), an immune-mediated disease of the central nervous system (CNS) characterized inflammation, demyelination, and axonal injury[24].

1.5 REBIF and DEAMIDATED VARIANT

Currently, several recombinant human interferonβ-1a (IFNβ-1a) formulation are commercially available for the treatment of MS. Among these, Rebif, was produced for the first time by Merck Company in 1986. It was approved by FDA in 1998 in Europe and in 2002 in USA. The first produced Rebif formulation was G1 with fetal bovine serum (FBS), a raw material included in the composition of the media used for cell expansion and bioreactor runs. Between 2005 and 2007, a new bovine serum-free and human serum albumin-free formulation, called G2, has been developed for Rebif. In particular, no FBS formulation was used during manufacture without human serum albumin (HBS) as an excipient, in order to reduce immunogenicity risk and improve tolerability. Indeed, this serum-free formulation of Rebif reduces the degree of neutralizing antibodies and it was finally approved in the EU for the treatment of relapsing MS, replacing the original formulation [25] [26].

This drug can be distinguished from another interferon commercially available, IFNβ-1b, based on structural differences that conversely depend on the recombinant technique of production. IFNβ-1b is the product of a bacterial expression system. It is obtained by cloning the molecule in *Escherichia coli* that are unable to glycosylate the recombinant protein, remove the N-terminal methionine during translation and replace one of the three cysteines with serine to maintain structural stability. Contrarily, recombinant IFNβ-1a is produced in eukaryote (Chinese Hamster Ovary) cell lines, it is N-glycosylated and it is identical to the natural form of human IFNβ.Chemical stability play a key role in the development of protein therapeutics due to its impact on both efficacy and safety. Specific amino acids represent "hotspots" residues that are subject to different chemical modifications, including glycosylation. Glycosylation has a complex impact on a wide range of molecule functions.

The lack of glycosylation leads to aggregation, thermal denaturation and a substantial decrease in the biological activity [27] .

The most abundant glycosylation pattern in CHO cell line is the complex-biantennary type. It consists of a conserved core structure composed by four N-acetyl-glucosamine (GlcNac) and three mannose (Man) units. This backbone can be further modified in Golgi apparatus by the addition of other sugars, as fucose (Fuc), galactose (Gal) and sialic acid (Neu), generating more complex glycoforms [28] (Figure 6). In particular, Rebif biantennary structure is characterized by the addition of two Neu, two Gal and one fucose units [29] [27] (Figure 6, in red).

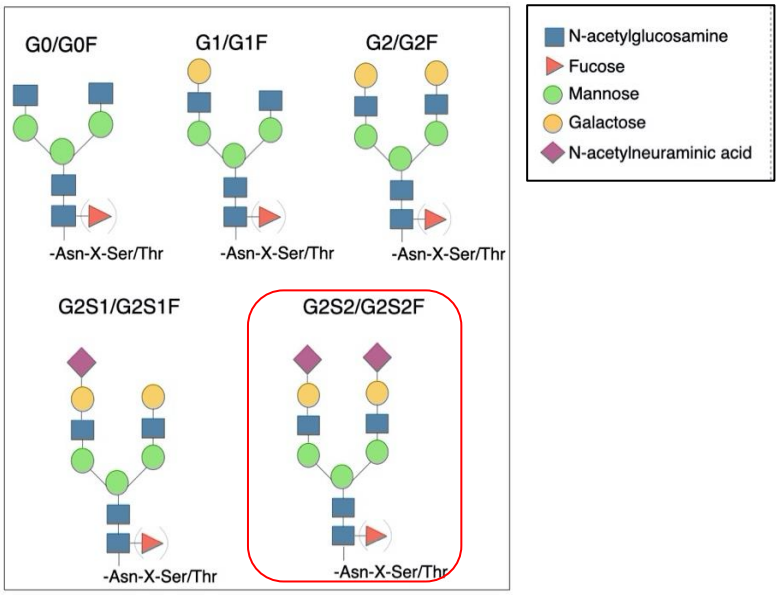

Figure 6.CHO N-glycosylation pattern. In red, Rebif biantennary glycoform includes one fucose unit, two N-acetylneuraminic acid (sialic acid) and two Galactose units. Image adapted from Immunoglobulin (IG) or antibody glycosylation [30].

The two formulation, IFNβ-1a and IFNβ-1b differ also for their biological activity. Both IFNβs share several immunomodulatory properties but show different antiviral activity. IFNβ-1a, due to the glycosylation, resulted more active than IFNβ-1b to eliminate viral infection [31] [24] [32]. However, glycosylation is not the only post-translational modification able to increase in biological activity. Preliminary data showed a greater biological activity of IFNβ-1a after artificial deamidation [33].

Deamidation has been reported to serve as a molecular clock for many biological processes including protein turnover and aging and it is one of the possible degradation routes of proteins [34]. This type of degradation occurs mainly at asparagine and glutamine residues.

However, not all asparagines in a protein are prone to undergo deamidation, depending on several factors among which the nature of the amino acid following the asparagine in the sequence (N+1 amino acid). Depending on the localization of the residue, deamidation could negative affect the biological systems unless it exerts a beneficial biological effect.

One differentiating factor of IFNβ from other type I interferon is the presence of a consensus sequence Asn-Gly (NG) for deamidation. Asn-Gly sequence is the most susceptible to deamidation, following by Asn-Ser sequence [33]. The deamidated variant is a human interferon-β protein analog in which the asparagine at position 25, numbered in accordance with native IFNβ-1a, is deamidated.

The primary structure of IFNβ-1a is reported in figure 7.

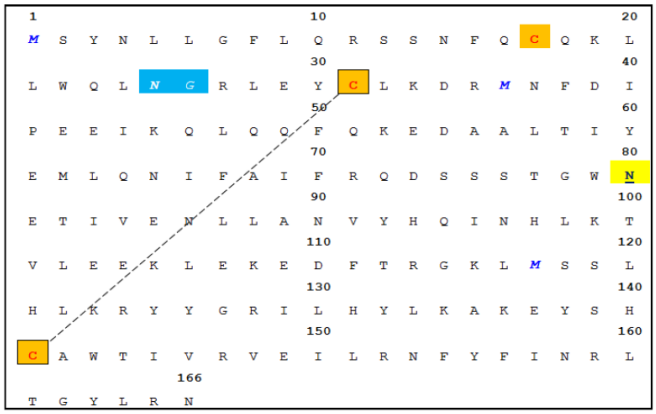

Figure 7.Human interferon beta-1a amino-acidic sequence. The N80 glycosylation site is underlined. Cysteine residues are in red. Disulphide bridge between C31and C141 is shown. Oxidable methionine residues are in blue italic. The Asn deamidation consensus sequence Asn25-Gly26 is blue box. Image adapted from https://www.uniprot.org/uniprot/B5BUQ5

For each asparagine undergoing deamidation, two possible degradation products are formed [35](figure 8):

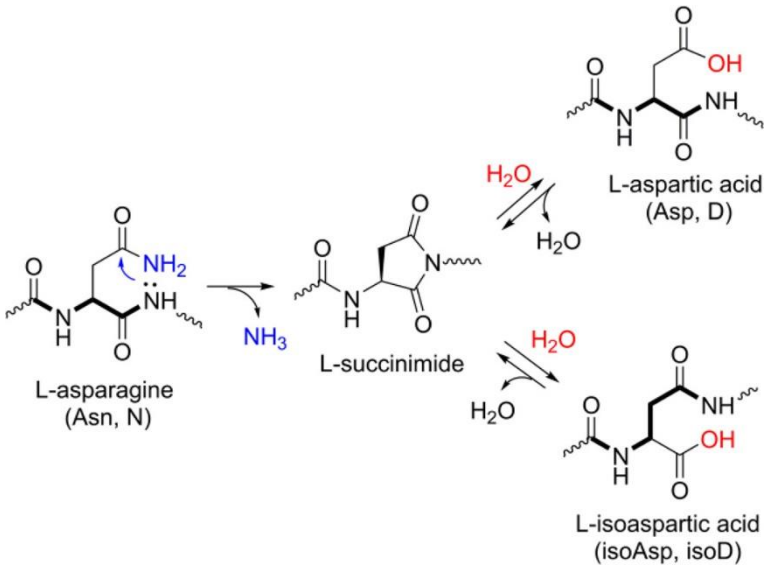

Figure 8. Deamidation of asparagine residues in proteins at neutral or alkaline pH. From "Mildly acidic conditions eliminate deamidation artifact during proteolysis: digestion with endoprotease Glu-C at pH 4.5" Liu et al. 2016 [36].

- The succinimide intermediate

  The peptide bond nitrogen (reactive anion) of the N + 1 amino acid binds the carbonyl carbon of the asparagine or aspartate forming the ring structure of a succinimide).

- The aspartyl and isoaspartyl protein

  The succinimide is rapidly hydrolyzed to form iso-aspartate (beta-aspartate) or aspartate.

The last two degradation products yield a change in the net charge of the protein, since the neutral amide side chain of the asparagine has been converted into the more acidic carboxyl group of aspartic acid.

Usually deamidation rate depends on several factors, among which pH, temperature and buffer composition[37]. High pH (pH 8-9) and temperature (>30°C) or some buffers could increase the deamidation rate as well as the deamidation extent. These factors affect the molecule integrity both during the production and purification as well as during the storage of drug substance and drug product. It must be highlighted that according to the spatial position of Asn25, its deamidation to Asp 25 is expected to increase electrostatic interactions with a spatially closed Arg147 with the possibility of forming additional hydrogen bonds with Arg147 and Thr144 [33].

Based on above consideration, Asn25 deamidation may contribute to stabilization of IFNβ-1a with an expected beneficial impact on thermal stability.

Indeed, as showed by Merck's previous studies, the IFNβ-1a deamidated product exhibits a higher stability but also an higher biological activity compared to its native form[33]. From a business perspective, due to the demonstrated higher biological activities, the deamidated variant of IFNβ-1a may have a therapeutic potential.

Several hypotheses have been proposed to explain the increasing biological activity of deamidated IFNβ-1a. First of all, the higher resistance against denaturation for the deamidated variant as evidenced by the chemical and thermal studies: several approaches was used to assess the level of deamidation, the monomeric purity of the protein, the structural stability as response to thermal and chemical stress and the potential impact of deamidation process on the secondary and tertiary structure [33].

All these tests show that the deamidation treatment bring to a complete molecule deamidation (about 95%). The distribution of the glycoforms, methionine oxidation and protein aggregation are not affected by the deamidation. Regarding the stability, melting temperature and Gibbs energy show that deamidated interferon is more stable, compared to its native form, at pH 3.8 than pH 7.2. Such differences cannot be responsible for the higher biological activity.

Literature data reports that a prolonged STAT1 activation or other signaling pathways could be involved in a different activity of IFNβ-1a deamidated form [15,38]. Only a complete molecule characterization can highlight the real mechanism involved in the higher biological activity of deamidated interferon beta.

1.6 THE ROLE OF BIOASSAY IN BIOPHARMACEUTICAL and LCM

Pharmaceutical companies use biological characterization to assess the quality, efficacy and stability of a product during all the drug's life cycle.

The characterization of a molecule includes a structural and a functional characterization. The first, uses physicochemical techniques to detect structural differences and post-translational or chemical induced modifications, while the second one uses specific bioassays for the assessment of the potency from the pre-clinical to the clinical phases and market [39].Potency can be defined as a quantitative measure of relevant biologic function based on the attributes that are linked to its clinical effect [40,41].

In this context, several methods have been developed to monitor and assess the biological activity of Rebif. Currently, the main Rebif biological activities are monitored using specific bioassays (Table 1) that include, in addition, the binding to its receptor IFNAR2. Each assay is developed using a definite system in order to better reproduce the biological MoA.

Activity	System
Antiproliferative assay	WISH cell line
Immunomodulatory assay	A549 cell line - MHC I expression
Antiviral assay	A549 cell line - EMCV
IFNβ receptor binding assay	Biacore-SPR

Table 1: Analytical procedure for biological characterization.

- The antiproliferative activity of IFNβ-1a samples was tested by determining the ability of interferon beta to inhibit the growth of the human amniotic cell line (WISH).
- The current immunomodulatory assay is based on the ability of IFNβ-1a to induce MHC I expression in A549 cell lines via cytofluorimeter.
- Antiviral activity was measured through a method based on the capability of IFNβ-1a to inhibit the cytopathic effect induced by vescicular stomatitis virus (VSV) in A549 cell line.
- Finally, Rebif binding affinity to its receptor is measure via SPR, monitoring the binding between IFNβ-1a and IFNAR2.

Moreover, bioassays can be used to establish comparability, test process intermediates and support product changes [42]. They are also a key part of establishing quality (ie, reproducibility and stability), which is critical to supporting the safety and efficacy profiles of biopharmaceuticals [43] and are necessary for regulatory submissions to support lot release [44].

The general process from drug development to its approval is defined and regulated by the Health Authorities: Food and Drug Administration (FDA) in US, European Medicines Assays (EMA) in Europe and Pharmaceuticals and Medical Devices Agency (PMDA) in Japan. Generally, the drug-development process from the drug discovery to marketed

product proceed through different clinical trial phases and it takes from 10 to up to 20 years [45].

The manufacture of a product requires modifications during the development phase as well as after its approval by the Health Authorities. For this reason, it is important the continuous monitoring and managing of the product to ensure its safety and quality over time[46].

This process is called Life Cycle Management (LCM) and it is important to control the product at all stages of its life to detect any changes in its quality and effectiveness.

Recently, an increasing interest for this concept exists also for analytical procedures. During the lifecycle of a drug product, both the manufacturing process and the analytical procedure can go through several changes because of continued improvement activities or the need to operate the method and/or process in a different environment. Applying a lifecycle approach to analytical procedures ensure updated methods aligned to the state-of-art of technologies and consequently the quality of the results. As these data are used as basis for decisions, their validity is extremely critical and they have to be able to provide these data in constant quality.

1.7 GENERAL APPROACH TO DEVELOP AND QUALIFY A BIOANALYTICAL ASSAY

The development of a new analytical method is drug-specific and the choice of the best assay depends from several factors. First, according to the Health Authorities, a good method should be representative of the specific MoA or effector function of the molecule that is going to be monitored for regulatory purposes.

Moreover, according to the ICH Q8 guidelines [47], the new developed method must be able to measure and control the critical quality attributes (CQAs) of the candidate drug.

CQA has been defined as "a physical, chemical, biological, or microbiological property or characteristic that should be within an appropriate limit, range, or distribution to ensure the desired product quality" [48] [49]. These critical quality attributes serve an important database for defining the drug properties during commercial production phase as well as post licensure life cycle management [50]. CQAs can vary based on post-translational modifications that can occur during different stages of the manufacturing process and for this reason they need to be defined and controlled during the developmental phases of a biologics [51]. The identification of product-specific CQAs is a regulatory requirement for market submission and they are identified by through a series of product risk assessment, usually performed in

early phase during pharmaceutical development process, based on clinical data, non-clinical data, prior knowledge with the molecule or other similar molecules and the published literature [52].

The approach to develop a method includes four main steps: 1) Bioassay identification, 2) Bioassay development and 3) method qualification 4) method validation [43]. This last step will not be described in this work.

- Bioassay identification

A bioassay could be optimal to reproduce the drug MoA but it could be costly to develop, perform, transfer and maintain. For this reason, identify the best assay is not always easy.

Unlike other analytical techniques, bioassays are almost always unique for each therapeutic. Cell-based assays are largely used to mimic the drug MoA. However, cell-based assays can be variable and can lack the precision and robustness of analytical methods due to the use of cells [43]. For this reason, in accordance with the regulators, a phased approach can be used to choose the appropriate assay. If the molecule is in an early phase of drug development, it is useful to start with binding methods such as Enzyme-linked immunosorbent assay (ELISA) and Surface plasmon resonance (SPR) technique but a more complex system using cell-based assays able to reproduce the drug's MoA must be developed for the late molecule phases. Indeed, a cell-based assay is always required to the product registration[39].In this context, all the Rebif related methods are cell-based assay except the binging to its receptor that serves as additional method to monitor the biological behavior.

In addition to the MoA, another aspect to consider for choosing a bioassay is its being "fit for use". Generally, a bioassay can be considered suitable for drug testing if it meets some requirements reported in several international guidelines [43,53]. To evaluate whether an assay is fit for use, analysts must clearly specify the purposes for performing the bioassay. For example, an assay could be used for a stability study, to establish the shelf life of the product, or for comparability/similarity studies.

- Bioassay development

Once identify the product's MoA and the method able to reproduce it, the bioassay development can start. The development of a cell-based assay begins with the selection or generation of a cell substrate that is usually the most critical reagent in a cell-based assay [43]. To obtain a robust assay other component are define such as the dose response curve, plate selection and layout.

- Cell line

The choice of appropriate cell lines with desirable amount of response and stability may be challenging and can influence the performance of the assay [39].This evaluation can be performed by verifying the expression of specific receptors on the cell surface and/or directly checking the response to the product. The cellular responses to the protein of interest depend on the drug's MoA and the exposure time. In Rebif bioassay, different cells type (e.g. A549, human non-small cell lung cancer) have been chosen for their ability to better represent the mechanism of action of interest.

- Dose response curve

Identify a correct dose response curve is one of the most important aspects of a method allowing to calculate the product potency. Bioassays usually show a nonlinear relationship between the response and the analyte such as log-concentration with a sigmoidal shape.
The 4-Parameters Logistic (4-PL) model is commonly used for curve-fitting analysis in bioassays or immunoassays [39].
As the name implies, it has 4 parameters that need to be estimated in order to "fit the curve". It is characterized by it's classic "S" or sigmoidal shape that fits the bottom and top plateaus of the curve, the 50% effective dose EC50, and the slope factor (Hill's slope). The 4-PL models consider the whole dose response range, resulting in the advantage that additional information about the asymptotes is given.
The 4-PL is described by the following equation:

$$Y = \frac{(A - D)}{\left(1 + \left(\frac{X}{C}\right)^{B}\right)} + D$$

where:

A = Minimum asymptote. In a bioassay where you have a standard curve, this can be thought of as the response value at 0 standard concentration. It is called bottom of the curve.

B = Hill's slope. The Hill's slope refers to the steepness of the curve. It could either be positive or negative.

C = Inflection point or ED_{50}. The inflection point is defined as the point on the curve where the curvature changes direction or signs. C is the concentration of analyte where Y=(A+D)/2.

D = Maximum asymptote. In a bioassay where you have a standard curve, this can be thought of as the response value for infinite standard concentration. It is called top of the curve.

A 4-PL function requires enough concentrations or dilutions to fit the model.

Several dose response strategies can be used but the ideal dose response curve is an eight or more dilution point well distributed for sigmoidal fits. In particular, at least one and preferably two dilution point are commonly used to define each asymptote (top and bottom of the curve) and three and preferably four dilution points in the linear part of the curve. For this purpose, a development objective would be to optimize experimental condition and step dilution to obtain a well-defined linear range. In this regard, the Hill slope (B parameter) value could help: if the concentration point are spatially well distributed and symmetric, the Hill slope value within the linear range is around 1 and this is the ideal condition to obtain a well-defined sigmoidal dose response curve [39].

Because of the inherent variability in test systems (animals, cells, instruments, and reagents), an absolute measure of potency is not possible. For this reason, during development phase, potency value is calculated using a relative quantification comparing Standard versus Standard to ensure the reliability of the data obtained. The Standard is a critical reagent in bioassays because of its quality as a reliable material to which a Test preparation can be quantitatively compared in a relative potency assay. Its potency is usually assigned a value of 1 (or 100%). The sample relative potency is obtained as the ratio of Reference EC50 to Test sample EC50. The reportable value is then calculated as the arithmetic mean from the corresponding samples replicate [54 39].

According to ICH <1032> guideline [43], potency can be measured only from samples that are similar to the standard and are within the range of the assay system. This means that both

the dose-response curves of sample and standard should have the common functional parameters (Hill slope and top and bottom asymptotes) and they should only differ by a horizontal curve-shift characteristic of a gain or loss of biological activity (Figure 9A). If P value is equal or bigger than 0.05, it means that the curves are similar, and the potency can be calculated. In contrast, if the curves parameters are dissimilar and parallelism is not met, the relative potency should be not reported as indication of biological activity. It happens when the horizontal displacement in not constant (Figure 9B), or when the top or the bottom of the curves have a different behavior (Figure 9C-D). This mean that the potency is not depends only from the horizontal shift between the two curves.

Consequently, considering the ratio between inflection point to calculate potency in not properly correct[39].

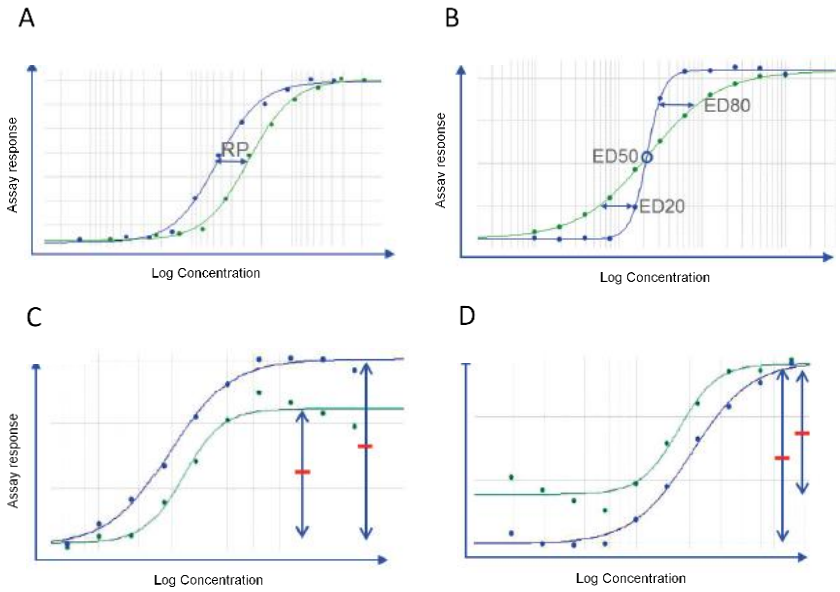

Figure 9.Dose-response curve and relative potency (RP) evaluation

- **Plate effect, assay layout and replicates**

Evaluate the plate effect mean to assess the homogeneity of the drug response in the plate. Find operating conditions for the assay is an important goal during development to avoid systematic effects across the plate.

To reduce the response variability through the plate is important to study the plate effect. Two main approaches are used to evaluate the plate affect. In the first, a single assay dose is used across all the plate. Then, the responses though the plate is evaluated comparing the value obtained in the external wells to those inside the plate.

The second approach uses a full-dose response range. In this case, the same reference material curve is added in the entire plate. In this case, only one curve is considered the reference material and the relative potency of the other samples is calculated on this.
Another approach to reduce the plate effect is the randomization. This is considered the best approach to minimizing the bias when its source is unknown. Indeed, the plate layout can be designed loading, in alternative row or columns, standard and sample in order to equally distribute the exposure to the edges. This plate design can help to protect against the so-called "row effects".
After identifying the appropriate layout for the assay, the choice of the number of replicates is another parameter to be evaluated. It may depend on the final assay application and on desired throughput and precision to be obtained. Commonly, at least two replicate intra-run for each sample and standard are employed.

- Method qualification

Once the approach for assessment has been defined, the experimental conditions of the bioassay must be standardized. For this purpose, the assay should be qualified to demonstrate that it is suitable for its intended purpose [55]. Method qualification is important to demonstrate the robustness of the assay under the experimental conditions in which will be performed. In general, the parameters evaluated during a qualification exercise refer to those described for validation and they include preliminary I) goodness of fitting, II) fold increase of the response, III) linearity and range, IV) accuracy, V) precision and VI) specificity. All these parameters are evaluated considering specific acceptance criteria defined in the guidelines [56].
Traditional measures of analytical goodness of fit include the R-square (coefficient of determination) of a curve comparing the theoretical concentration to the signal from the method.
R-square determines how well the sample curve fit the 4-PL algorithm and its value ranges from 0.0 to 1.0. The closer R-square is to 1, the better the curve fit the model. Usually, an R-square $\geq$0,95 is used as acceptance criteria for this parameter.
The fold increase of the response is determined as ratio between the top and the bottom of the Standard curve and it should be a value greater than 3.

According to ICH Q2 (R1) [56], linearity of an analytical procedure is its ability (within a given range) to obtain test results which are directly proportional to the concentration (amount) of analyte in the sample (Figure 10). The range of an analytical procedure is the interval between the upper and lower levels of analyte (including these levels) that have been demonstrated to be determined with a suitable level of precision, accuracy, and linearity.

For the establishment of linearity, ICH recommends a minimum of 5 concentrations and a minimum specified range from 80% to 120% of the test concentration. The specified range is normally derived from linearity studies and depends on the intended application of the procedure [57].

Accuracy and precision are other two analytical performance characteristic that should be considered during method qualification. Accuracy of an analytical procedure is the closeness of test results to the true value (Figure 10). The accuracy of an analytical procedure should be established across its range and it is expressed as recovery percentage of known amount of added analyte [57]. Traditional measures of analytical recovery percentage are between 75% and 125% and it is calculated as follow: % recovery = (measured concentration/standard concentration) *100.

The Precision of an analytical procedure expresses the closeness of agreement (degree of scatter) between a series of measurement obtained from multiple sampling of the same homogeneous sample under the prescribed conditions (Figure 10). The precision of the method was measured in terms of CV (Coefficient of Variance) for each percentage calculated: % coefficient of variance (CV) = (√Variance of replicate component /mean) *100. It should be a value equal or less than 25 %.

It is a measure of repeatability and reproducibility of the analytical procedure under normal operating condition [57].

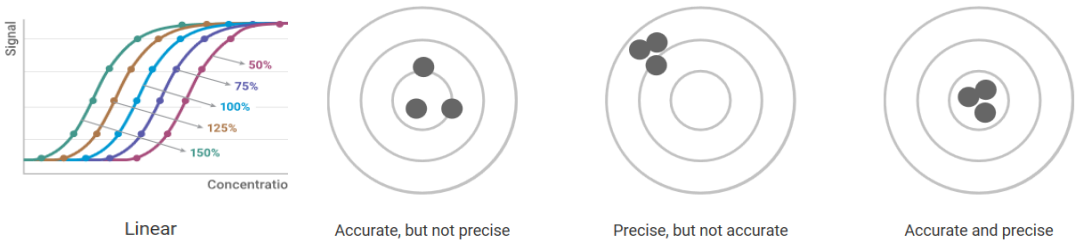

Figure 10: Analytical performance characteristic: Concept of linearity, accuracy and precision.
https://ita.promega.com/applications/biologics-drug-discovery/bioassay-qualification

Regarding specificity, the ICH documents define it as the ability to assess unequivocally the analyte in the presence of components that may be expected to be present, such as impurities, degradation products, and matrix components [57].

There are two ways to demonstrate method specificity: first, it must able to measure the specific analyte and not some other protein or substance. Second, it must show bias in presence of interfering compound or matrices.

Once verify all the above described parameters, the developed method can be considered qualified and can be used for non-GMP testing.

If a method fail qualification, it gets re-optimized until it can achieve acceptable performance or it is rejected for the intended application.

2 AIM

The purpose of this work is the hunt of the mechanism involved in the higher biological activities of deamidated IFNβ-1a and its additional MoAs. In order to start a dedicated R&D project and be considered as a new biological entity, the mechanism underlying such higher MoAs have to be fully explored. For this reason, an investigation on the deamidated sample has been carried out and different approaches, from *in silico* to *in vit*ro assays, were applied to understand suchs effects. The biological activity of deamidated IFNβ-1awas previously assessed by applying specific bioassays that are part of the Rebif characterization analytical panel. However, these bioassays were developed many years ago and, due to the relevant methods variability, a comparison might have been not accurately provided. For this reason, two new cell-based assays mimicking the mechanisms of action (MoA) of the drug has been developed and qualifiedto monitor and characterize the biological activity of the deamidated moleculeensuring accurate and precise results. In order to identify the mechanism underlying the greater biological response of the deamidated IFNβ-1a, the activity of the canonical IFNβ-1a pathway, receptor binding affinity and IFNAR-IFNβ-1a interaction network has been evaluated. Moreover, with the aim to possibly explore other therapeutic areas and foster the product knowledge about the yet unknown potential of the drug, the scouting of new possible IFNβ-1a MoAs has been carried out.

3 MATERIALS AND METHODS

IFNβ-1a Drug substance (DS)

Highly purified IFNβ-1aG1 drug substance (DS) was supplied by Merck. The production method used a recombinant expression of the protein in a CHO-K1-derived cell line using a commercial serum-free medium. Crude harvests were processed through a series of chromatographic steps, which included affinity, ion exchange, reversed-phase and size exclusion chromatography. The final drug substance was formulated and stored in sodium acetate with a pH of 3.8. The IFNβ-1aG1 drug substance (DS) concentration is 0,367 mg/mL.

IFNβ-1a deamidation

The artificial deamidated interferon was prepared by incubating IFNβ-1a G1 DS sample into 1.2M Ammonium Bicarbonate pH 9.2 at +5ºC for 18 hours. The deamidation buffer was then removed by ultrafiltration through Amicon Ultra 10k and buffer exchanged with Sodium Acetate buffer pH 3.8.After deamidation process, deamidated variant andIFNβ-1a G1 DS concentration was verified measuring the absorbance at 280nmvia nanodrop considering Rebif molar extinction coefficient (ε). The concentration of deamidated variant and IFNβ-1a G1 DS is 0,328 mg/mL and 0,270 mg/mL, respectively.

Immunomodulatory assay

The immunomodulatory assay is based on the ability of interferon beta-1a to upregulate the MHC class I expression on the A549 cells in a dose-related manner. A549 cell line is received from ATCC. Cells were cultured at 37°C ±0.5°C, 5% CO_2in DMEM(1X) + GlutaMAX (Gibco cat. 31966-021) in presence of 10% Fetal Bovine Serum (FBS, Fisher scientific cat. 10270) and 1% penicillin and streptomycin antibiotics (Gibco, cat. 15140-122). When adherent cells have reached 80% confluence, they were detached with trypsin (Euroclone cat. ECB3052D) and re-suspended in culture médium at $0{,}65x10^6$ cells/mL. 50µL/well of this cellular suspension was added in a black 96 well plate. Cells were treated with IFNβ-1a reference material and deamidated variant dilution curve in a range from 200 ng/mL to 0.000102 ng/ml and incubated at 37°C ±0.5°C, 5% CO_2 for 48h. After incubation

time, a blocking buffer (3%BSA in DPBS) was added in the plate for 30 minutes. Cells were washed in DPBS (Gibco cat.14040-091) and a Monoclonal Anti-HLA Class I-Biotin antibody (Sigma cat. SAB4700638) was added into the plate for 1 hour. After incubation, 3 washes steps were performed and the Streptavidin PE (eBioscience cat.12-4317) was added in the plate for 30 minutes. Finally, cells were washed for the subsequent analysis to the plate reader. Three independent analytical runs were performed for each experiment. Data analysis was made using Graph Pad Prism software. IFNβ-1a concentrations (X values) are Log10 transformed and the analytical response (Y value) expressed as FI. The dose response curve of IFNβ-1a reference material and samples are fitted by 4PL and the IFNβ-1a concentration able to induce the MHC I expression in A549 cell line at 50% of the maximum possible (EC50) is automatically calculated using the GraphPad-Prism software. The potency of each samples has been calculated as the ratio of reference EC50 to sample EC50.

Antiviral reporter Gene assay (AVA RGA)

The antiviral reporter gene assay measures the upstream phase of the antiviral response by evaluating the activation of the luciferase reporter gene. ISRE-luc2P/HEK293 cell line, purchased by Promega (manufacturer code CS190701), has been used as target cell. These cells are transfected with a plasmid containing the firefly luciferase gene under the control of the Interferon Stimulated Response Element (ISRE) and hygromycin resistance gene. The binding of IFNβ-1a to IFNAR, activates the JAK/STAT signalling pathway and induces the translocation of the ISGF3 complex to the nucleus and the binding to the ISRE element. The activation of ISRE element leads the activation of the luciferase gene not involving the use of the virus. Target cells were grown in DMEM High Glucose medium supplemented with FBS (Fisher scientific cat. SH3007103) and Hygromycin b (Invitrogen cat. 10687010) (the antibiotic used for the stable clone selection) as for the manufacturer instruction. To measure IFNβ-1a antiviral activity, ISRE-luc2P/HEK293 were detached with Trypsin EDTA 0.25% (Gibco cat. 25200-056) and resuspended in culture medium. $2x10^4$ cells/wells were added in a white plate (assay plate) and incubated for 2 hours (pre-plating incubation

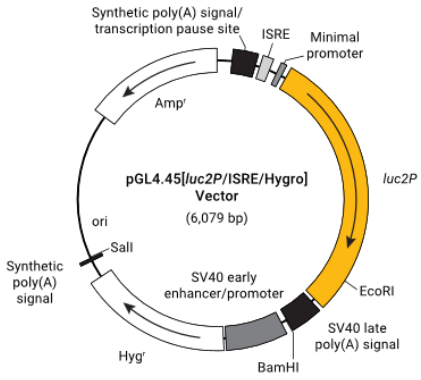

step) at 37°C ±0.5°C, 5% CO_2 ±0.5Then, cells were treated with IFNβ-1a reference material and deamidated variant dilution curve in a range from 50 ng/mL to 0.003 ng/mL and incubated at 37°C ±0.5°C, 5% CO_2. After 24 hrs, the BioGlo Reagent was added to the plate and the emitted luminescence with a Luminescence counter was measured. Data analysis was performed using Graph Pad Prism software. Three independent analytical runs are performed for each experiment. IFNβ-1aconcentrations (X values) are Log10 transformed and the analytical response (Y value) expressed as RLU. The dose response curve of reference material and samples were fitted by 4PL.The Interferon concentration able to induce the Luciferase expression on ISRE-luc2P/HEK293 at 50% of the maximum possible (EC_{50}) was automatically calculated using the GraphPad -Prism software. The potency of each samples was calculated as the ratio of reference EC50 to sample EC50.

STAT1 phosphorylation

A549 cells were grown as described previously. When cells reached 80% confluence, $3x10^4$ cells/well were seeded in a 96 well plate and incubated overnight at 37°C with 5% CO_2. After incubation time, cells were treated with 0,02 ng/mL of deamidated IFNβ-1a and its native form for 15minute at 37°C with 5% CO_2. Untreated cells were used as control. Then, A549 has been washed in PBS and the Alpha SureFire Ultra Multiplex assay kit (PerkinElmer, cat. MPSU-PTERK-K-HV) has been used to lyse the cells and measure both the phosphorylated and total levels of endogenous STAT1 protein in cellular lysates. The Alpha Multiplex measurement was carried out in the same assay plate well from a single sample of cell lysate and was achieved by the use of two types of Alpha Acceptor beads that emit at distinct wavelengths (545nm and 615nm). The two distinct Alpha Acceptor beads report their binding to a distinct antigen through their association with specific assay antibodies, as indicated below:

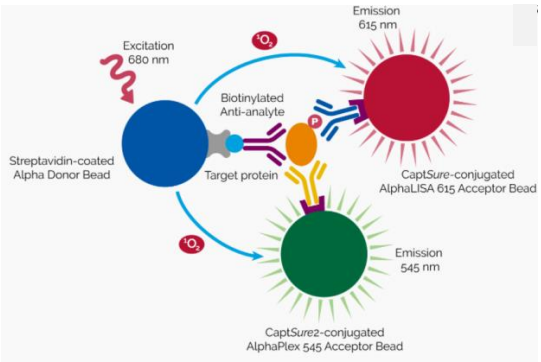

The 615nm (Europium) signal corresponds to the phosphorylated protein analysis while the 545nm (Terbium) signal correspond to the total STAT1. An AlphaScreen protocol was used to read the plate via Envision plate reader. The results were shown as average of three independent experiments performed in duplicate and normalized on the untreated cells.

Real time qPCR

A549 cells were cultured in DMEM(1X) + GlutaMAX (Gibco cat. 31966-021) in presence of 10% Fetal serum bovine (FBS, Fisher scientific cat. 10270) and 1% penicillin and streptomycin antibiotics (Gibco, cat. 15140-122). When cells reached 80% confluence, they were harvested and $1x10^4$ cells/well were seeded in a 96well plate and incubated 1h at 37°C with 5% CO_2. After incubation, cells were exposed to 0,02ng/mL of IFNβ-1a and its deamidated variant for 24h at 37°C with 5% CO_2. Cell lysis step and the real time qPCR were performed using the Fast Lane Cell Multiplex kit (QIAGEN cat 216513). For Real Time PCR, all genes were evaluated with taqman chemistry on a 7500 Fast Real Time PCR instrument.

Primer used for RT-PCR are reported below:

- MX1Thermo fisher scientificHs00895608_m1 cat.4453320
- CCR1 Thermo fisher scientificHs00174298_m1 cat.4331182

The cyclic parameters were as follow:

Step	**RT**	**Polymerase activation**	**Denaturation**	**Extension**
Time	20’	15’	45’’	45’’
Temperature	50°C	95°C	94°C	60°C
Cycle number	1	1	40	

Data are obtained from three independent experiments performed in triplicate. The expression levels of the target genes relative to that GAPDH (Thermo fisher scientific cat 4326321E) were determined using the comparative CT method (fold change in target genes relative to untreated samples= $2^{-\Delta\Delta CT}$

SPR analysis

In SPR analysis, the ligand of interest is immobilized on the chip surface through a commonly applied chemistry. Different concentrations of the analyte are flown over it to characterize its interactions to the immobilized ligand. Monitoring the change in the SPR signal over time produces a sensorgram, a plot of the binding response (RU) versus time. Fitting the sensorgram data to an appropriate kinetic binding model allows calculation of kinetic parameters, such as the association (ka) and dissociation (kd) rate constants, and the binding affinity of the tested interactions. The binding affinity, defined as the of protein-protein interactions is typically measured and reported by the equilibrium dissociation constant (KD), which is used to evaluate the strengths of biomolecular interactions. The smaller the KD value, the greater the binding affinity of the ligand for its target. The larger the KD value, less the target molecule and ligand are attracted to each other.

- ***Binding to IFNAR2***

The interactions between IFNβ-1a/IFNAR2was performed by surface plasmon resonance (SPR) with the Biacore 200 instrument. The binding surface was created by the capturing of IFNAR2 via monoclonal Ab (Mab) to IFNAR2 (Merck, MS-T clone 35.9) previously immobilized to a CM-dextran surface (CM5 sensor chip, Biacore cat. BR-1005-30) by ammine coupling chemistry. Mab anti IFNAR2was injected over the chip with a flow rate of 5µL/min and 5min of injection time. Then, IFNAR2 (25nM; flow rate: 20 µL/min; injection time: 2.5 min) was injected over the MAb in the measurement flow cell, while reference flow cell was used as blank control. A range of five IFNs concentrations (50, 25, 12.5, 6.25, 3.125 nM) were flown over the chip in a multi cycle kinetic, injecting each concentration at 75 µl/min. At the end of each cycle the chip surface was regenerated by injection of Glycine pH 2.5 solution at 20µL/min for 30s. Before each sample, a blank cycle was performed running the Running buffer (HBS-EP, GE cat. BR-1001-88) instead of the Interferon concentration range, that was then subtracted to the sample curve in the

elaboration phase. Sensorgram data were processed and fitted using BIA evaluation software. The sensorgram was produced plotting the time (s) (on X axis) versus the binding response (RU) (on Y axis).Quantitative analysis of IFNβ-1a samples binding to the IFNAR2 was performed applying the 1:1 binding model. The equilibrium dissociation constant (KD) was estimated as well as the association and dissociation rate (ka and kd, respectively). SPR/Biacore results characterizing the IFNAR2 interaction with each ligand were expressed as absolute KD and relative binding (%KD). Each KD value was obtained from the average of three independent experimental runs while the %KD was obtained from the ratio percentage of IFNβ KD to deamidated sample KD.

- ***Binding to IFNAR1***

The His/Nickel layout, chosen to study IFNβ-1a/IFNAR1 interaction via Biacore 200, is based on the His/Nickel chelating reaction. An NTA chip, coated with nitrilotriacetic acid (NTA), was activated with a Ni^{2+} solution. 0,25µg/mL of His-tagged IFNAR1 protein (SinoBiological cat 13222-H08H) was captured via its His-tagged tail only on the Measurement Nickel activated flow cell, while the Reference flow cell remains empty as blank control.

A range of five IFNβvariants concentrations (22, 15, 7.5, 3.75, 1.875 nM) were flown over the chip in a single cycle kinetic, injecting each concentration at 30 µl/min for 180 s. The dissociation phase was monitored flowing the buffer for 600 s at 30 µl/min. At the end of each cycle the chip surface was regenerated by injection of an EDTA 0.35 M solution at 30µL/min for 60s.Before each sample, a blank cycle was performed running the Running buffer (HBS-P+, GE cat.BR-1006-71) instead of the Interferon concentration range, that was then subtracted to the sample curve in the elaboration phase. Three independent analytical runs have been performed. Sensorgram data were processed and fitted using BIA evaluation software. The sensorgram was produced plotting the time (s) (on X axis) versus the binding response (RU) (on Y axis). The association and dissociation constant (ka and kd, respectively) and the absolute KD were estimated applying the 1:1 binding model.

Sensorgram Comparison

This comparability software tool, with its *Similarity Score,* provides a means to quantitate differences/similarities in binding. *Sensorgram Comparison* relies on comparison of kinetic data of samples against that of a defined reference standard. In this tool, a standard deviation corridor, representing the experimental variation of IFNβ-1a (control sample), was calculated. Sample binding data with high similarity to their control sample should be found within the standard deviation (SD) corridor. For both IFNAR1 and IFNAR2 binding experiment, two representative runs were used (two replicates of reference material and two for the samples). The resulting files were all opened in *Sensorgram Comparison* and a standard deviation corridor, representing the upper and lower limits of experimental variation, was calculated to obtain the sample's similarity score based on the number of data point inside and outside the SD corridor.

Alphascreen for IFNβ-1a/IFNAR proximity evaluation

The AlphaScreen method parameters used to measure the binding of interferon beta to its receptor subunit IFNAR1 and IFNAR2, is briefly described below:

Layout	
AlphaScreen Acceptor Beads	coated with Protein A
AlphaScreen Donor Beads	Nickel
Ligand	IFNAR1-HisTag and IFNAR2-Fc Tag
Analyte	IFNβ and deamidated variant
Curve layout	Horizontal; 10 points

Interferon native and deamidated variant were prepared at 20 µg/mL, with serial dilution of 1:2 for 10 points in immunoassay buffer (Perkin Elmer cat. AL000C) and added to the alpha assay plate. IFNAR1-HisTag (Sino Biological cat.13222-H08H) and IFNAR2-Fc Tag (Sino Biological cat. 10359-H02H) were prepared as mix at 6µg/mL and added to IFNs curves. Finally, beads mix (Protein A Alpha Donor beads, AS102D and Nickel Chelate AlphaLISA Acceptor Beads, AL108C; PerkinEkmer) was prepared at 10 µg/mL and added in alpha

assay plate. The plate was incubated for 1h at 25°C in the dark. After incubation, the plate was read using AlphaScreen protocol provided by Envision software. IFNs concentrations (X values) are Log10 transformed and the analytical response (Y value) expressed as CPS. The dose response curve of IFNβ-1a and Deamidated variant were fitted by 4PL and the IFNs concentration able to induce the binding to IFNAR at 50% of the maximum possible (EC_{50}) was automatically calculated using the GraphPad-Prism software. However, due to the rejection of the null hypothesis obtained by the software, it was not possible calculate the potency. For this reason, the binding affinity was calculated as drug efficacy using the ratio of the Top value obtained from Graphpad software.

In Silico analysis: Homology modeling

The three-dimensional (3D) structure of IFNAR1::IFN-β::IFNAR2 ternary complex was built by a chimeric homology modeling approach, using the "Homology model" tool by MOE 2019.01 software (Molecular Operating Environment, Chemical Computing Group, Montreal, QC, Canada) [58] . The crystallographic structure of the IFNAR1::IFN-ω::IFNAR2 complex (PDB ID: 3SE4)[12] and the X-ray structure of IFN-β (PDB ID: 1AU1) [8] were used as a template to model receptors and to orient IFNβ in the correct binding mode. Both templates were prepared by the "Structure preparation" module to fill sequence gaps, correct any crystallographic issues and add missing hydrogens in order to adjust residues protonation states. 10 intermediate models were obtained and the final structure was selected basing on the best-scoring intermediate one. The score was computed according to the Generalized Born/Volume Integral (GB/VI) methodology [59]. An energy minimization step was carried out for the final model until the root mean square (RMS) gradient reached a value of 0.5 kcal/mol/Å^2. Starting from this structure, G2S2F glycans were manually attached to the Asn80 residue by the "Carbohydrate builder" and the final glycosylated model was optimized by a further energy minimization (RMS gradient 0.01 kcal/mol/Å^2). A second model of the complex with the N25D mutation in the IFN-β molecule was built by introducing the single amino acid substitution *via* the "Protein builder" tool. The mutated model was then further minimized until the RMS gradient reached a value of 0.01 kcal/mol/Å^2. All the calculations in the modeling procedure were performed with the AMBER10:EHT force field [60] and the Reaction field (R-field) was applied to treat electrostatics contribution [61,62]. Hierarchical clustering analysis uses an algorithm that

groups similar objects into groups called clusters. By using hierarchical clustering one conformation per each complex was extracted from the trajectory. Specifically, three groups of conformations were identified in each system and the centroid structure of the most populated groupwas considered to analyze the 3D structure of the complex.

In silico analysis: Molecular dynamics simulations

A molecular dynamics (MD) simulation 500 ns long was carried out for both wild type and deamidated complexes by NAMD 2.13 package [63]. In both systems, before the MD production phase, an energy minimization was run for 5000 steps, followed by 100 ps of heating and 20 ns of equilibration. The simulations were performed in the NVT ensemble, so by considering constant number of particles, constant volume and constant temperature (T=300 K). The Langevin thermostat was used to set constant temperature and the Langevin piston was used for pressure control. Each protein in the complex was capped at N- and C-terminus with an acetyl (ACE) and an N-metyl amide (NME) group, respectively. Both systems were solvated by TIP3P solvation model and centered in a rectangular periodic water box of the following XYZ dimensions: 120.97 Å X 98.54 Å X 79.76 Å (wild type system) and 129.5 Å X 106.2 Å X 88.1 Å (deamidated system). NaCl 0.1 M was added for system charges neutralization. The sample time was set to 10 ps and the integration time step to 2 fs. The system preparation was performed by MOE GUI (Graphical User Interface). All the trajectory analyses were carried out by MDtraj [64] and MOE.

MAPK phosphorylation

A549 cells were grown as described previously. When cells reached 80% confluence, $2x10^4$ cells/well were seeded in a 96 well plate and incubated overnight at 37°C with 5% CO_2. Cells were treated for the established time (5-15-30-60min) with 50ng/mL of IFNβ-1a and IFNβ-1a deamidated variant. Following the treatments, cells were washed with phosphatase-buffered saline and the MAPK Family (ERK, p38, JNK) Activation InstantOne ELISA kit (Thermo Fisher Scientific, cat. 85-86195) was used to lyse the cells and measure ERK, P38 and JNK phosphorylation, as suggested by the supplier's manual. The absorbance was measured using a colorimetric plate reader set at 450nm. The results were shown as average

of three independent experiments performed in duplicate normalized on the untreated (CTRL).

NF-kB phosphorylation

To evaluate NF-kB phosphorylation, the NFkB p65 (Total/Phospho) Human InstantOne™ ELISA Kit (Thermo Fisher Scientific, cat. 85-86083-11) was used. A549 cells were grown as previously described. Cells at 80% confluence were harvested and $2{,}5x10^4$ cells/well were seeded in the 96well plate supplied by the kit. After 1 h of and pre-incubation at 37°C with 5% CO_2, cells were treated for the established time (30min) with 20ng/mL of IFNβ-1a and its deamidated variant. Following the above treatments, cell lysis and antibodies provided by the kit were used to lyse the cells and measure NF-kB phosphorylation. The absorbance was measured using a colorimetric plate reader set at 450nm. The results were shown as average of two independent experiments performed in duplicate normalized on related control and total NF-kB.

Proteomic analysis

A549 cells were grown as previously described. Cells at 80% confluence were harvested and $0{,}5x10^6$ cells/well were seeded in the 6 well plate, treated with 1ng/mL of IFNβ-1a and its deamidated variant and incubated at 37°C with 5% CO2 for 24h. Then, cells supernatant has been collected.

Precipitation techniques was proposed to concentrate the sample and remove small interfering species, such as salts & detergents. Acetone precipitation is a common method for precipitation and concentration of protein. Three mL of each compound were prelevated and under were with acetone[65].To get protein identification, the resulting proteins underwent trypsin-catalyzed in digestion procedure (Promega, Milano, Italy). NanoUPLC-hrMS/MS analyses of the resulting peptides mixtures were carried out on a Q-Exactive orbitrap mass spectrometer (Thermo Fisher Scientific), coupled with a nanoUltimate300 UHPLC system (Thermo Fisher Scientific). Peptides separation was performed on a capillary BEH C18 column (0.075 mm × 100 mm, 1.7 μm, Waters) using aqueous 0.1% formic acid (A) and CH3CN containing 0.1% formic acid (B) as mobile phases and a linear gradient from 5% to 50% of B in 90 minutes and a 300 $nL \cdot min^{-1}$ flow rate. Mass spectra were acquired over

an *m/z* range from 400 to 1800. To achieve protein identification, MS and MS/MS data underwent Mascot software (v2.5, Matrix Science, Boston, MA, USA)[66] analysis using the non-redundant Data Bank UniprotKB/Swiss-Prot (Release 2020_03). Parameter sets were: trypsin cleavage; carbamidomethylation of cysteine as a fixed modification and methionine oxidation as a variable modification; a maximum of two missed cleavages; false discovery rate (FDR), calculated by searching the decoy database, 0.05. The data analysis of protein was carried out using the gene ontology tool in the UniProtKnowledgebase[67].

Statistical analysis

Where indicated, significance was analyzed using One Way Analysis of Variance (ANOVA). Significance was defined at $*p < 0.05$, $**p < 0.01$, $p*** < 0.001$. Paired samples statistical analysis was used to compare two method performance. If the standardized skewness and standardized kurtosis obtained are inside the range of -2 to +2 means that no significant deviations from normality has been found.

4 RESULTS

4.1 DEVELOPMENT OF A CELL-BASED ASSAY MEASURING MHC-I EXPRESSION

The development of a cell-based assays, measuring the capability of Rebif to induce MHC I expression via plate reader, was needed to compare the deamidated IFNβ-1a to its native form. The goal has been to reach high performances in terms of precision, accuracy and throughput. The whole development phase was performed comparing Reference Standard versus itself. The cell number and incubation time has been taken as starting point by the method formerly applied but that revealed higher variability. In particular, at the end of a feasibility step, A549 cell line has been used as cellular model for the assay and treated for 48h with IFNβ-1a to measure MHC I expression. Starting from this format, other parameters has been assessed and reported below:

	Tested parameters
1	Plate type
2	Dose response curve
3	Layout
4	Antibodies
5	Buffer

Table 2: New immunomodulatory assay tested parameters

A black 96 well plate was used in the plate reader format to reduceautofluorescence and consequently background signal. In order to obtain a better sigmoidal shaped-curve with a fold increase higher than 3, different concentrations range and step dilutions of IFNβ-1a reference material were evaluated in combination with different fluorescent antibodies (Ab) (Figure 11A).In detail, starting from the feasibility IFNβ-1a concentration range (1000 ng/mL to 0,000512 ng/mL), an anti-MHC I antibody (AbI) recognized by a FITC-labelled secondary antibody (FITC-AbII) was tested using several primary antibody concentrations (Figure 11A; curve 1, 2). Subsequent experiments (Figure 11A; curve 3-6) were performed testing different IFNβ-1a concentration ranges with a biotin-streptavidin system: a primary anti MHC-I biotin antibody recognized by a labelled streptavidin was evaluated (biotin-AbI

+ strept PE). In this phase also the assay buffer has been adjusted. The use of BSA+DPBS buffer is used in several bioassays to reduce no specific signal and it was tested for the plate reader format. Moreover, a vertical layout was evaluated in curve 5 (Figure 11A) aiming to increase the throughput. The dose-response curves, generated applying the parameters abode described, were reported in figure 11B. The fold increase was calculated for each curve as ratio between top and bottom of the relative dose response curve. All the conditions showed a fold-increase < 3 except for the curve5 and 6 (Figure 11C). The main differences in these two curves were the horizontal versus vertical layout and a different IFNβ-1a concentration range. Both curves, obtained using a biotin-streptavidin system and the BSA-PBS buffer, were chosen for the evaluation of the plate effect in order to finally decide the best performing condition. The other curves (curves 1-4) were discarded.

A

Curve	IFNβ-1a concentration range	Antibody	Layout	Buffer
1	1000 ng/mL to 0,000512 ng/mL	1:100 AbI + 1:100/1:200 FITC-Ab II	Horizontal	FBS+DPBS
2	1000 ng/mL to 0,000512 ng/mL	1:100 AbI + 1:100/1:50 FITC-AbII	Horizontal	BSA+DPBS
3	1000 ng/mL to 0,000512 ng/mL	1:100/1:300 biotin-AbI + strept PE	Horizontal	BSA+DPBS
4	1000 ng/mL to 0,000128 ng/mL	1:100 biotin-AbI + strept PE	Horizontal	BSA+DPBS
5	40ng/mL to 0,000512 ng/mL	1:100 biotin-AbI + strept PE	vertical	BSA+DPBS
6	200 ng/mL to 0,0001024 ng/mL	1:100 biotin-AbI + strept PE	Horizontal	BSA+DPBS

B

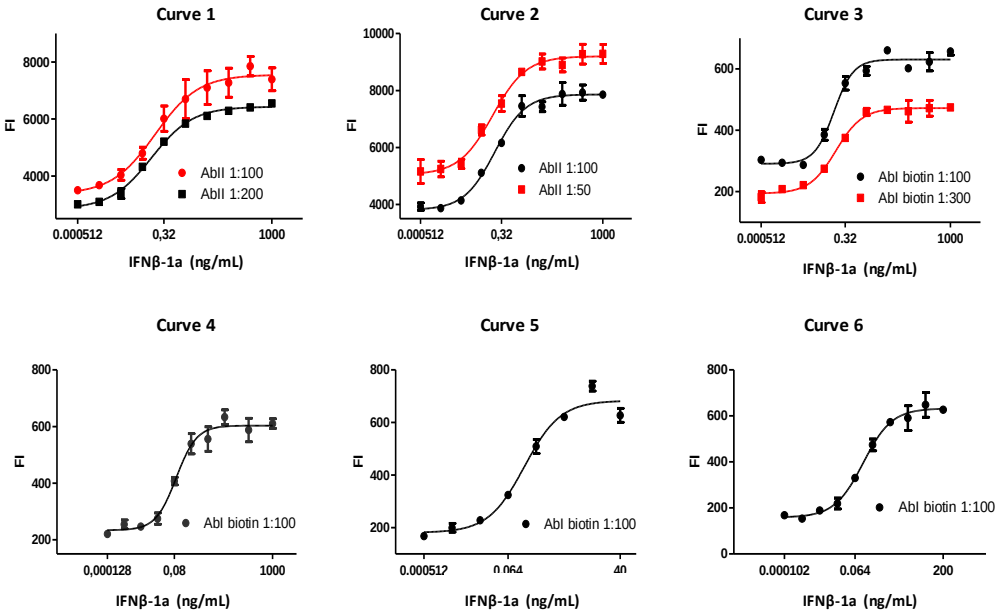

C

	Curve 1		Curve 2		Curve 3		Curve 4	Curve 5	Curve 6
	1:100	1:200	1:100	1:50	1:100	1:300			
Fold increase	2,2	2,3	2,1	1,8	2,2	2,4	2,6	3,8	4

Figure 11. ***A)*** *Black 96 well plate: conditions explored. AbI: anti-MHC I primary antibody; FITC-AbII: FITC-labelled secondary antibody; biotin-AbI: Biotin-labelled primary antibody; Strept PE: streptavidin conjugated with phycoerythrin (PE).* ***B)*** *IFNß-1a reference material dose-response curves of explored conditions (n=1).* ***C)*** *Fold increase of each dose-response curve tested as described in A).*

4.1.1 Plate effect

The plate effect of the curve 5 and 6 was evaluated during the bioassay development step to guarantee the uniformity of response throughout the plate. A randomization approach was used. A549 cell line were treated with curve 5 and 6of IFNβ-1a reference material for 48h. Then, MHC I expression was assessed using the biotin-streptavidin system. In detail, the IFNβ-1areference material was analysed in 8 concentration points (curve 5, vertical layout) and 10 concentration points (curve 6, horizontal layout) testing different format. A representative dose response curve (Figure 12A) and the table containing the results of relative potency (Figure 12B) of the best format chosen for each curve have been reported below. Data were fitted by 4PL algorithm considering as triplicates the values coming from columns 1-5-9, 2-6-10, 3-7-11, 4-8-12 (curve E) and from lines b-d-f, c-e-g (curve F). The relative potency was calculated considering the sample in column 1-5-9 (curve E) and line b-d-f (curve F) as the reference material. The main difference between curve 5 and 6 was the number of samples tested per plate (one sample for curve 6 and three samples for curve 5). The number of internal replicates was unchanged (three internal replicates). Although curve 5was the preferred layout for the number of possible tested samples, it showed a high variability intra-assay in all tested formats (data not shown for 1-2-3; 1-2 format) and the proposals have been rejected. The curve 6 showedthe uniformity of response throughout the plate with b-d-f, c-e-g formatand less variability within the internal replicates. Considering the results obtained in the feasibility study, this layout was selected to qualify the method. In Figure 12C, the optimized parameters for the new immunomodulatory assay were summarized. The whole method outline was described in Material and Method section.

A

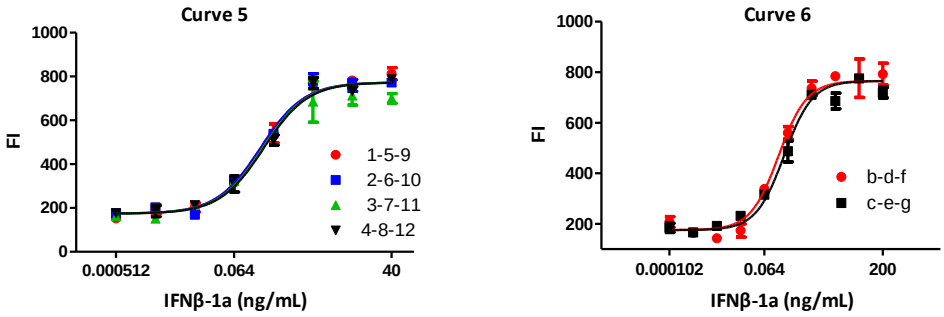

B

Curve 5

	Potency		
Run	**2-6-10**	**3-7-10**	**4-8-12**
1	102	152	104
2	101	116	135
3	108	156	93
average	**104**	**141**	**111**
CV%	4	16	20

Curve 6

	Potency
Run	**c-e-g**
1	112
2	88
3	80
average	**93**
CV%	18

C

	Plate reader format
Concentration range	200ng/mL to 0.0001024 ng/mL
Type of well	Black 96well
Layout	Horizontal
Buffer	BSA in DPBS
Primary antibody	Biotin anti-HLA
Detection	Streptavidin-PE
Method	Plate reader

*Figure 12. **A)** Dose response curves showing representative 1-5-9 (curve 5) and b-d-f (curve 6) layout. To calculate the potency, red curve was considered as reference material while the other one as sample. **B)** Relative potency obtained from each layout was calculated as ratio of Reference EC50 to Sample EC50. Three independent analytical runs have been performed for curve 5 and 6. **C)** Selected parameters for the plate reader format.*

4.1.2 Immunomodulatory assay method qualification

Once the main method parameters have been defined, the performances of the optimized bioassay were evaluated according to the ICH guideline. During the development study, the performance of the Rebif immunomodulatory assay was evaluated as a preliminary i) goodness of fitting, ii) linearity, iii) precision and iiii) accuracy. To consider the method qualified, the obtained values must meet the acceptance criteria reported in Figure 13A.

The goodness of fitting of a dose-response curve is evaluated in terms of coefficient of determination (R^2) and determines how well the IFNβ-1a curve fits the 4PLalgorithm. R^2 values calculated in all the bioassays performed during the development study were collected and used to estimate a preliminary goodness of fitting. Results were reported in Figure 13B.The R^2 was found to be ≥ 0.95, a value closer to 1.0, confirming that the developed Rebif dose-response curve properly fits the 4PL algorithm.

In order to calculate linearity and range, interferon beta reference material was tested at five different percentage of his nominal concentration. The potency was calculated as ratio between EC50 of each different interferon percentage concentrations (50%,75%,125% and 150%) to the EC50 of the 100% concentration of the reference material. Finally, linearity was calculated as the interpolation of the potency data obtained on a straight line (figure 13C). Based on the CV requested by acceptance criteria, the reference material tested at 150% of the nominal concentration showed a CV $\geq$ 25 % and it was not accepted. Based on this results, immunomodulatory assay showed a linearity range between 50% and 125% (0,5-1,25 potency ratio) with the R^2 of the linear regression curve equals 0.9758.

Preliminary precision and accuracy were estimated from the experiments run in the linearity study.

As shown in figure13D, in a range of potency between 50%-125%, the accuracy of the method was found between 97%÷109%.

The precision of the method was measured in terms of CV (Coefficient of Variance) for each percentage calculated. The maximum value obtained in the analytical range (50%-125%) was found to be equal to 21% (figure 13D).

Both the preliminary Precision and Accuracy values were found within the acceptance criteria (Figure 13A,D).

A

Parameter	Acceptance criteria
Goodness of fit	$R^2 \geq 0,95$
Linearity	– R^2-value ≥0.95; – CV≤ 25% in each concentration point
Accuracy	– Recovery= 75 - 125 %;
Precision	CV≤ 25%

B

Exp. No.	R^2	Exp. No.	R^2	Exp. No.	R^2	Exp. No.	R^2	Exp. No.	R^2
1	0,9967	13	0,9909	25	0,9762	37	0,9973	49	0,9923
2	0,9869	14	0,9875	26	0,9916	38	0,9817	50	0,9926
3	0,9904	15	0,9521	27	0,9916	39	0,9695	51	0,9905
4	0,9721	16	0,9833	28	0,9956	40	0,9857	51	0,9835
5	0,9949	17	0,9995	29	0,9907	41	0,9994	52	0,9887
6	0,9895	18	0,9949	30	0,9969	42	0,9792	53	0,9949
7	0,9892	19	0,9943	31	0,9935	43	0,9966	54	0,9937
8	0,9898	20	0,9974	32	0,9513	44	0,9962	55	0,9909
9	0,9974	21	0,9983	33	0,9853	45	0,9953	56	0,9960
10	0,9978	22	0,9984	34	0,9865	46	0,9994	57	0,9906
11	0,9961	23	0,9973	35	0,9983	47	0,9937	58	0,9942
12	0,9777	24	0,9954	36	0,9992	48	0,9924	59	0,9943

C

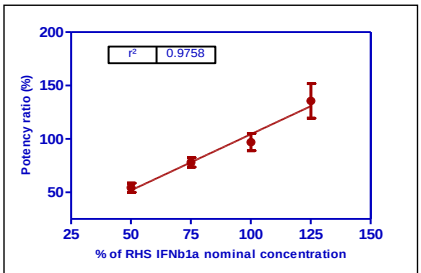

	Potency Ratio %				
Exp	50	75	100	125	150
Average	54	78	97	136	176
Recovery	108	104	97	109	117
%CV	14	10	14	21	32

D

Goodness of fit	$R^2 > 0,95$
Linearity	50-150%, $R^2 = 0,9758$
Accuracy	97-109
Precision	21%

*Figure 13. **A)** Acceptance criteria for each parameter tested during preliminary. **B)** R^2 values calculated in all the bioassays performed during the development study were collected and used to estimate a preliminary goodness of fitting. **C)** Preliminary linearity of the reference material tested in a range between 50%-150% of the nominal concentration. **D)** Summary of the value obtained from each method qualification parameters. All of them met the acceptance criteria.*

4.1.3 Bridging study

The immunomodulatory method, developed and qualified as shown, met all the acceptance criteria. In order to demonstrate the method suitability to measure the activity of interferon and possibly determine differences between different batches with better performances than the method used in the past, a bridging study has been performed. For this purpose, a set of six IFNβ-1a DS samples, previously analyzed with the FACS-based method (data not shown), was tested with the new assay. All samples were tested in three independent analytical runs and the biological activity of IFNβ-1a is expressed as % activity over the current reference material (Table 3). Finally, the obtained results were statistically compared to those of FACS based assay to demonstrate the similarity between the methods. For this purpose, a paired samples statistical analysis was applied. Standardized skewness and kurtosis value were within the range expected for data from a normal distribution showing no significative differences between methods (Table 3).The closeness to the target expected for the tested DS material shows a higher level of accuracy.

Sample	FACS-based method	Plate reader format
	Potency (%)	Potency (%)
1	97	97
2	88	100
3	101	91
4	95	105
5	88	99
6	85	101
Stsnt skewess	1,2	
Stnt kurtosis	0,3	

Table 3. Method comparability. The biological activity (potency %) of six IFNβ-1a DS samples tested with both methods were reported. Standard skewess and kurtosis were found within the similarity range (-2 to +2) confirming the method comparability.

4.2 DEVELOPMENT OF AN ANTIVIRAL REPORTER GENE ASSAY

As anticipated, (see paragraph 1.6), the antiviral activity of IFNβ-1a has been measured using a virus-based method. Since the disadvantages of this assay (use of virus, time consuming and variability), a new cell-based assay able to measure the IFNβ-1a (G1 and G2 clones) antiviral effect has been developed. For this purpose, an Antiviral Reporter Gene Assay (AVA RGA) was designed for monitoring the activity of Type I interferon induced JAK/STAT signalling pathway in the cultured cells. To evaluate the antiviral activity of interferon beta, ISRE-luc2P/HEK293 has been chosen as target cells. This cell line is stably transfected with a plasmid carrying the luciferase as reporter gene under the control of ISRE promoter. The development study was divided in two steps:

1) the selection of the properly described dose response curve (dose-response curve evaluation)

2) method optimization

4.2.1 Dose response curve evaluation

During feasibility step, several IFNβ-1a reference material dose response curve were tested using the parameters described in Figure 14A. A vertical layout and 24h of pre-plating and

incubation time were assessed. Among all IFNβ-1a concentration tested (data not shown), only curve 1 and curve 2 showed well described dose-response curve (Figure 14B). In curve 1, an IFNβ-1astarting concentration at 50ng/mL and a 1:4 step dilution was used to obtain the dose-response curve. Differently, a 20ng/mL of IFNβ-1a reference material was used as starting concentration in the curve2 and a 1:3 step dilution was used to build the dose response curve. Both the approaches properly describe the reference standard biological behavior. However, curve 1 is characterized by a well-defined top and bottom plateau and it was selected for the method optimization and qualification.

A

Parameters	
Target cells	ISRE-luc2P/HEK293
Number of cells/well	10000
Pre-plating incubation time	24 hrs at 37°C, 5%CO2
Bioassay incubation time	24 hrs at 37°C, 5%CO2
Curves layout	Vertical, 8 points

B

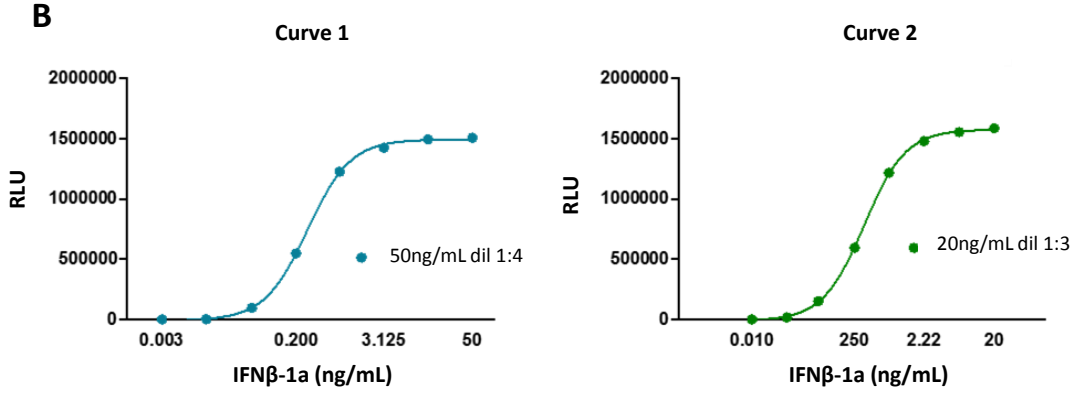

*Figure 14. **A)** Starting AVA RGA parameters using in feasibility phase. **B)** Dose response curve obtained from different IFNβ-1a starting concentration and step dilution (n=1).*

4.2.2 AVA RGA method optimization

Upon the best-dose response curve determination, the method optimization was performed. The parameters evaluated in the optimization stage were described in Table 4 with the aim to reduce the incubation times and to guarantee the higher method throughput. Indeed, the main goal of this step was to test more samples in the shortest possible time. Two incubation phases named as "bioassay incubation time" and "pre-plating incubation time" were

assessed. The first refers to the cell incubation time after IFNβ-1a treatment. The second one refers to the time in which the cells remain on the plate before treatment.

Critical Parameters
Bioassay incubation time
Number of target cells/well
Pre-plating incubation time
Plate effect

Table 4. Critical parameters tested during optimization phase

Starting from the condition selected during the feasibility step, curve 1was tested by modifying the time of interferon incubation time (3 hours or 6 hours instead 24hours) leaving unchanged cells number (10000 c/w) and pre-plating incubation time (24h). The obtained results indicate that 3h of incubation time have a strong impact on the bioassay while 6h incubation is not sufficient to obtain a well described dose response curve, with the loss of the bottom of the curve (Figure 15A). Based on this result, the incubation time was considered a critical step for this method and was not possible strongly modify it. For all these reasons, the condition selected for the bioassay incubation time was 24h. Since was not possible to change the bioassay incubation time, a decrease of pre-plating incubation time was evaluated with the aim to improve the easyness of the method. First, no pre-plating and a different number of cells per well was analysed to verify if this parameter was critical for the bioassay. As shown in Figure 15B, the number of cells per well was a critical parameter for the method. In the tested condition, the best signal and described dose-response curve were obtained seeding 20000 cells per well, that was indeed selected as the cell density parameter for the bioassay. The dilution points of the dose response curve obtained without pre-plating incubation time were not well distributed in the curve. For this reason, pre-plating was increased and tested at 2hrs, maintaining unchanged cell number and IFNβ-1a concentration range. The obtained results showed that 2h of pre-plating incubation was sufficient to obtain a suitable described dose response curve (Figure 15C). This condition was selected as pre-plating incubation time of the assay. In conclusion, all the tests performed allowed to optimize the method, by reducing the pre-plating incubation time (from 24 hours to 2 hours) and setting the cell density to 20000 cells per well. Considering

all the results obtained during the method optimization, the parameters reported in figure 15D were finally selected for this assay.

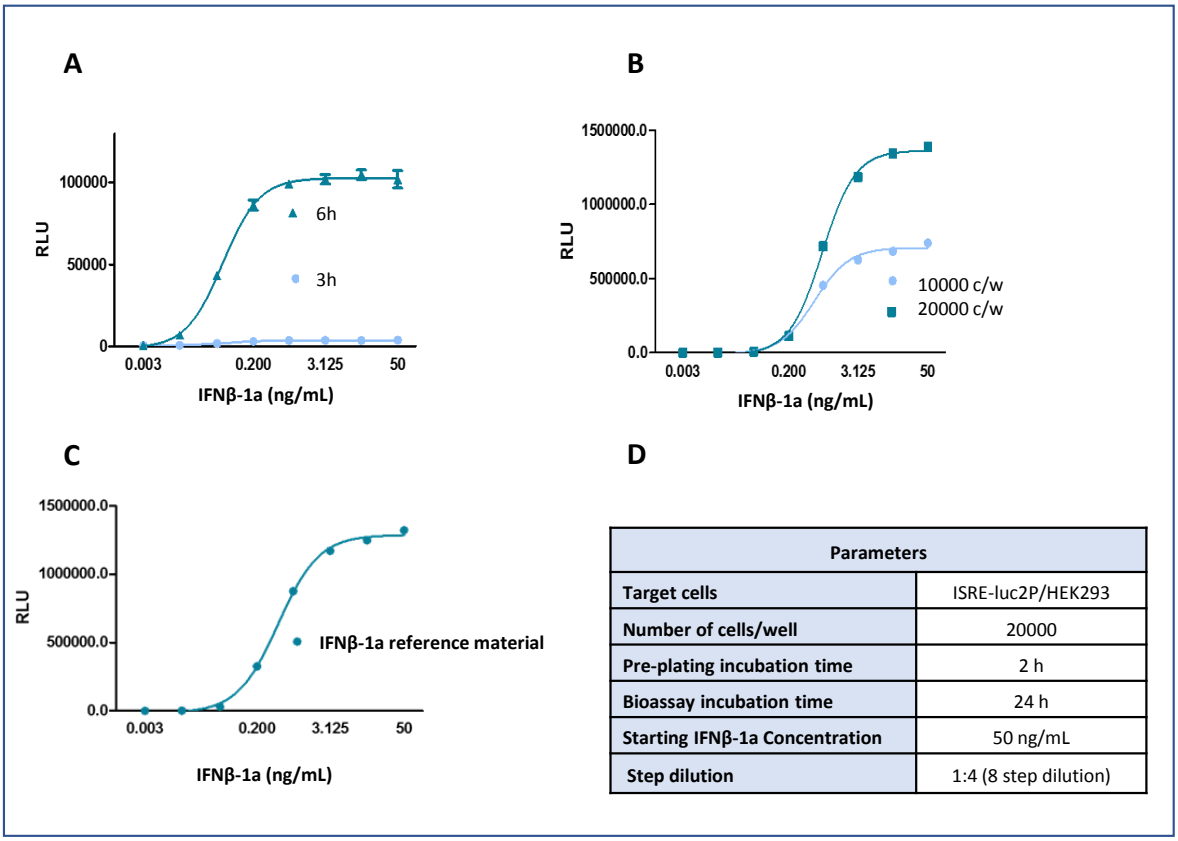

Parameters	
Target cells	ISRE-luc2P/HEK293
Number of cells/well	20000
Pre-plating incubation time	2 h
Bioassay incubation time	24 h
Starting IFNβ-1a Concentration	50 ng/mL
Step dilution	1:4 (8 step dilution)

Figure 15. AVA RGA method optimization. ***A)*** *10000 c/w were seeded, pre-plated for 24h and subsequently treated with IFNß-1a Curve 1. Bioassay incubation time was evaluated at 3h and 6h (n=1).* ***B)*** *10000 and 20000 c/w were seeded and directly treated with IFNß-1a Curve 1 (No pre-plating) (n=1).* ***C)*** *20000 c/w were seeded and incubated for 2h. After pre-plating incubation time, cells were treated with IFNß-1a Curve 1 (n=1).* ***D)*** *Parameters selected for the antiviral RGA.*

4.2.3 Plate effect

In order to guarantee the uniformity of the response throughout the plate, the plate effect was evaluated during the bioassay optimization step.IFNβ-1a reference material has been analysed in 8 concentration points. To verify if the selected layout could be affected by the sample position into the plate, reference material dose response curve was tested using the whole plate withdifferent layouts (1-2;1-2-3;1-5-9). Sample in column 1-2; 1-2-3 and 1-5-9 respectively was considered as reference material. Relative potency and CV% were calculated for each layout. Considering the results in terms of shape of dose response curves, potency, and CV% of the tested layout, the layout 1-5-9 showed a lower CV% and the uniformity of the response in the whole plate and it was selected for the qualification of the method (Figure 16).

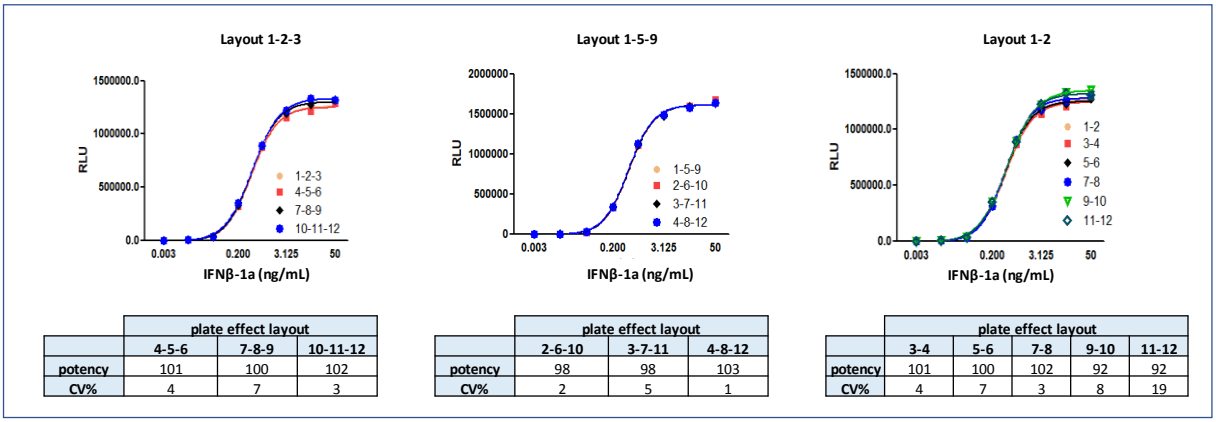

	plate effect layout		
	4-5-6	7-8-9	10-11-12
potency	101	100	102
CV%	4	7	3

	plate effect layout		
	2-6-10	3-7-11	4-8-12
potency	98	98	103
CV%	2	5	1

	plate effect layout				
	3-4	5-6	7-8	9-10	11-12
potency	101	100	102	92	92
CV%	4	7	3	8	19

Figure 16. Plate effect evaluation. Representative dose response curve for each tested layout has been reported. Three independent analytical runs have been performed for each condition. Potency was calculated as ratio percentage of Reference EC50 to Test sample EC50.

4.2.4 AVA RGA method qualification

Once developed the method, a qualification in terms of goodness of fitting, linearity, precision and accuracy has been evaluated according to the ICH guideline. The acceptance criteria to be met are shown in Figure 13A.The goodness of fit was evaluated through the R^2 value measured in all the experiments carried out during the development study. All R^2 values of the reference material, tested at 100% of the nominal concentration, generated within this study have been collected (figure 17A). All results are ≥ 0.98, demonstrating the goodness of fitting of the applied model.

In order to evaluate assay linearity, IFNb-1a reference Material was tested as a sample at 50%, 71%, 100%, 141%, 200% of the nominal concentration and the potency for each point has been calculated. Finally, linearity range was calculated as the interpolation of the potency data obtained on a straight line (figure 17B). All the linearity acceptance criteria have been met. Antiviral RGA showed a linear range between 50% and 200% with the R^2 of the linear regression curve equals 0.9758. As shown in Figure 17C, the accuracy of the method in the range of potency tested was found between 97%÷104% while the preliminary precision in term of CV% was found 9%. All the tested parameters met the acceptance criteria described in Figure 13A. Based on these results, the antiviral assay can be considered qualified.

A

Exp. No.	R^2	Exp. No.	R^2
1	0,9880	16	0,9985
2	0,9922	17	0,9980
3	0,9891	18	0,9981
4	0,9880	19	0,9982
5	0,9967	20	0,9995
6	0,9966	21	0,9975
7	0,9977	22	0,9964
8	0,9971	23	0,9994
9	0,9983	24	0,9985
10	0,9982	25	0,9982
11	0,9986	26	0,9981
12	0,9989	27	0,9983
13	0,9981	28	0,9964
14	0,9976	29	0,9996
15	0,9946	30	0,9983

B

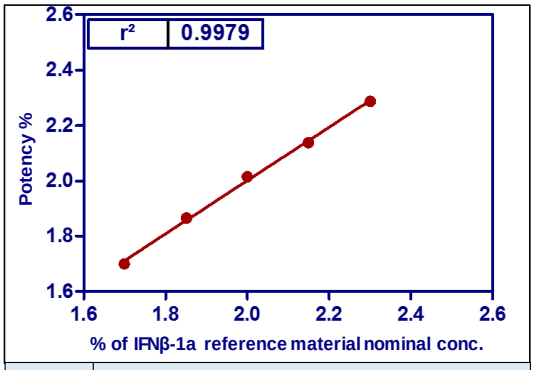

	Potency Ratio %				
	50	71	100	141	200
Average	50	73	104	137	194
Recovery	100	103	104	97	97
%CV	8	9	9	1	3

C

Goodness of fit	R^2 > 0,95
Linearity	50%-200%; R^2 = 0,9979
Accuracy	97%-104%
Precision	9%

*Figure 17. **A)** R^2 values calculated in all the bioassays performed during the development study were collected and used to estimate a preliminary goodness of fitting. **B)** Preliminary linearity results of the reference material tested in a range between 50%-200% of the nominal concentration. **C)** Summary of the value obtained from each method qualification parameters. All of them met the acceptance criteria.*

4.3 DEAMIDATED IFNβ-1aBIOLOGICAL ACTIVITY

Once AVA RGA and immunomodulatory assays have been developed and qualified, both were used to accurately and precisely evaluate the potency of the deamidated sample in order to confirm the literature data. Indeed, as mentioned in paragraph 1.5 of this work, previous studies have shown a higher biological activity of the deamidated IFNβ-1a compared to the native form. For this purpose, deamidated sample was produced from IFNβ-1a DS G1 sample using parental procedure as described in material and method section. Deamidated variant has been tested against IFNβ-1a DS G1, considered as reference material. Each sample was analyzed using both cell-based assays in three independent runs applying the criteria defined during the methods development and described in material and method. First,

the antiviral activity of deamidated sample was evaluated. ISRE-luc2P/HEK293 cell line was treated with a concentration range from 50 ng/mL to 0.003 ng/mL of deamidated and native IFNβ-1afor 24h. As reported in figure 18 A-B, the potency of the deamidated versus control was found to be 207%, 2-fold compared to the untreated interferon beta.

The same approach was used for the immunomodulatory assay. Deamidated sample effect was compared against the untreated IFNβ-1a to evaluate a different immunomodulatory activity. In this experiment, A549 cell line were exposed to deamidated/native IFNβ-1atreatment (concentration range from 200 ng/mL to 0.000102 ng/ml) for 48h and MHC I expression was measured. In figure 18, a representative dose response curve and the relative results were reported. Also in this case, the deamidated sample showed an higher biological activity compared to IFNβ (2-fold) (figure 18 C-D).

Based on the obtained results, both developed methods, AVA RGA and immunomodulatory assay confirmed the higher biological activity of deamidated IFNβ-1a. Moreover, in the case of starting dedicated R&D projects, the methods are already qualified for the purpose. The fitness for purpose, together with high precision and accuracy have been demonstrated.

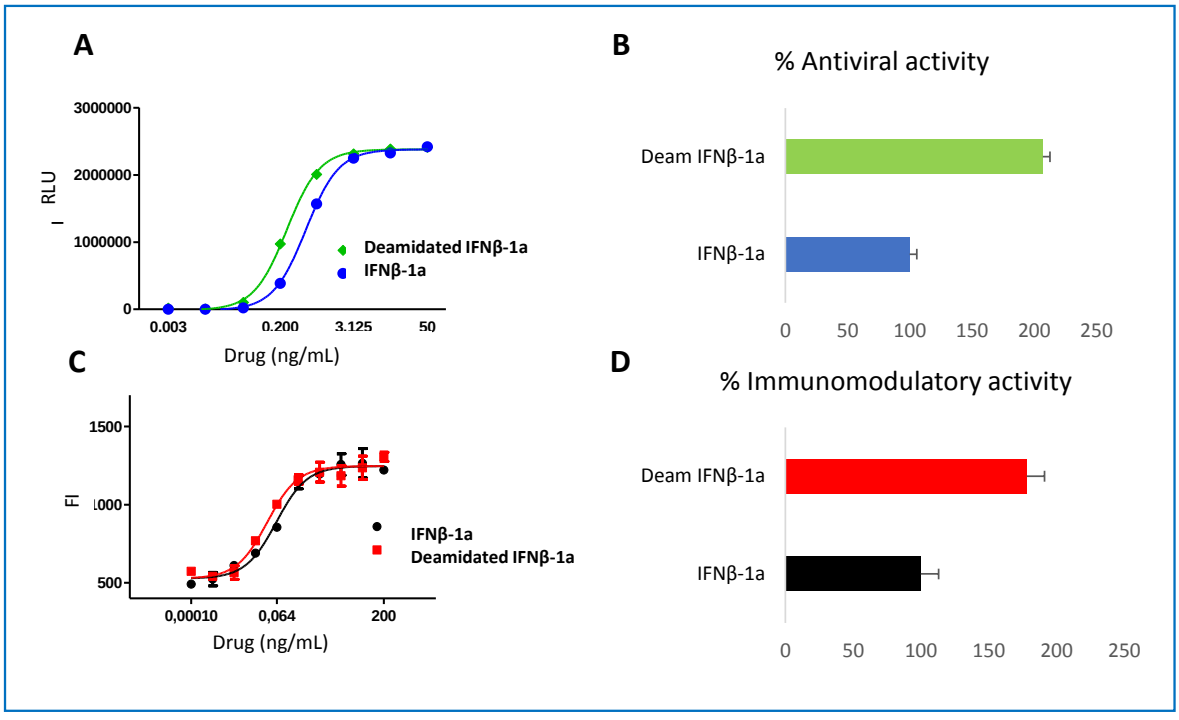

*Figure 18. In vitro antiviral **(A-B)** and immunomodulatory **(C-D)** bioactivities of deamidated IFNβ-1a compared to untreated control (IFNβ-1a). In both antiviral and immunomodulatory assay, cells were treated with IFNβ-1a variants for 24h and 48h respectively. In figure **1A** and **1C** the obtained dose response curves after interferon exposure were reported for each assay. In figure **1B** and **1D** the related potency, calculated as the ratio percentage of reference IFNβ-1a EC50 to deamidated sample EC50, has been graphically reported. Three independent analytical runs were performed applying the criteria defined during the methods development.*

4.4 STAT1 PHOSPHORILATION AND ISGs EXPRESSION

Once the increased biological activity of deamidated variant has been confirmed, the mechanism underlying this effect has been studied. Since A549 cell line was previously used to demonstrate the increased biological activity of IFNβ-1a, these cells were chosen as target cells. First, the activity of the canonical IFNβ-1a pathway was evaluated to assess the involvement of the conventional signaling in the observed cellular responses. In particular, STAT1 phosphorylation and ISGs target gene expression were evaluated. STAT1 phosphorylation has been measured in A549 cells after 15min of deamidated interferon treatment in comparison with native IFNβ-1a. As shown in Figure 19A, Interferon variants affect phospho-STAT1 differently. While IFNβ-1a slightly increases STAT1 phosphorylation, it is highly phosphorylated following deamidated IFNβ-1a treatment. In particular, deamidated variant increases STAT1 activity up to ~70% compared to the untreated (Control) and ~ 40% compared to native IFNβ-1a. Then, the expression of ISGs was assessed to evaluate whether the higher STAT1 activation, induced by deamidated IFNb-1a, correlates with an increased target gene expression. For this purpose, the expression of MX1 and HLA-C, two genes involved in antiviral and immunomodulatory activity respectively, have been evaluated after interferons exposure via Real Time qPCR. As shown in Figure 19B, both MX1 and HLA-C genes are upregulated in A549 cells when exposed to native and deamidated IFNβ for 24h. Interestingly, deamidated IFNβ increases significatively both genes expression of ~2-fold compared to the native form. These results show a greater effect of the deamidated variant on the JAK-STAT signaling pathway compared to the native IFNβ-1a.

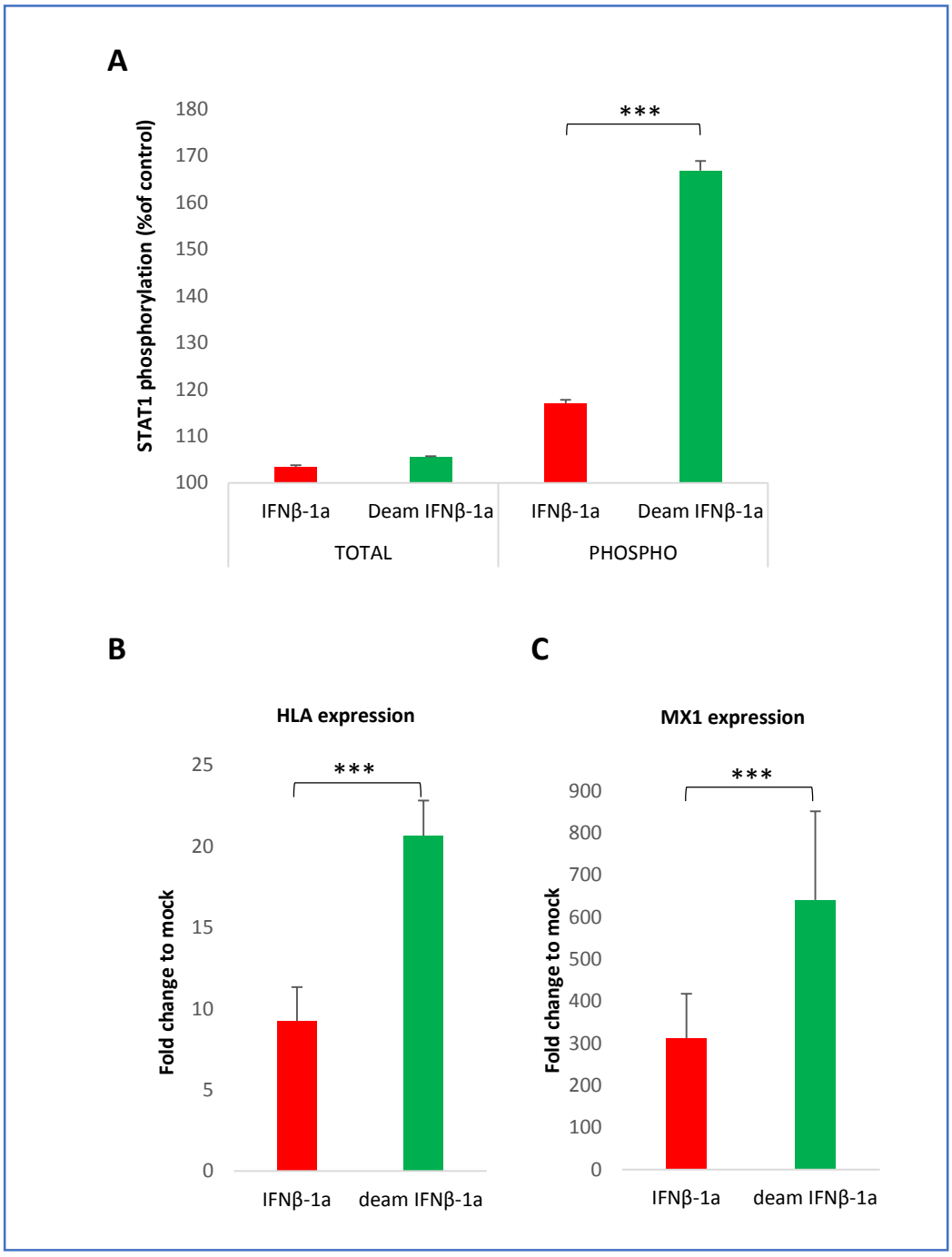

Figure 19. ***A)*** *Total and phospho-STAT1 under interferon variants treatment. A549 were treated with 0,02ng/mL of native and deamidated interferon beta for 15min. After treatment, cells were lysed and the amount of total and phosphorylated STAT1 has been measured.* ***B-C)*** *MX1 and HLA gene expression after interferon exposure. A549 cells were incubated with 0,02ng/mL of native and deamidated Interferon beta. After 24h, cells were harvested for Real Time qPCR. Data were from three independent analytical runs. All results are presented as Standard Error Mean (SEM). ***p <0.001 as determined by one-way ANOVA.*

4.5 BINDING AFFINITY TO IFNAR2

In order to explain the higher genes expression and consequent biological activity related to deamidated IFNβ-1a treatment, the binding affinity to IFNAR was investigated. In physiological condition, IFNβ-1a binds with high affinity IFNAR2 and low affinity IFNAR1. For this reason, a higher affinity of deamidated IFNβ-1a to IFNAR2 has been hypothesized as the obvious cause of the observed effect. To confirm this hypothesis, a SPR method was used.

In this method layout (Figure 20A), IFNAR2 was captured on the sensor chip by an anti-IFNAR2 antibody. The same concentration range (50, 25, 12.5, 6.25, 3.125 nM) of deamidated IFNβ-1a and its native form (used as reference material) were separately injected over IFNAR2 to measure each KD. The sensorgrams obtained from each interferon interaction to IFNAR2 are shown in Figure 20B. The binding affinity of deamidated interferon beta to IFNAR2 is given in terms of relative binding (KD%), calculated as ratio percentage of IFNβ KD value to deamidated sample one. Surprisingly, the deamidated sample shows a higher KD value resulting in a lower affinity (81%) to IFNAR2 compared to its native forms (Figure 20C). To assess if this difference was statistically significant, a one-way ANOVA analysis was performed between interferon native and deamidated sample. A p value = 0,02 was found confirming the lower affinity of the deamidated interferon to IFNAR2. Focusing on IFNβs kinetic constants, the dissociation rate played a key role on the different interaction profile of the deamidated IFNβ-1a. Indeed, the ka of deamidated and native IFNβ-1ais very similar, while a higher dissociation rate (kd) characterizes the deamidated sample resulting in a reduced affinity to IFNAR2 (Figure 20D).

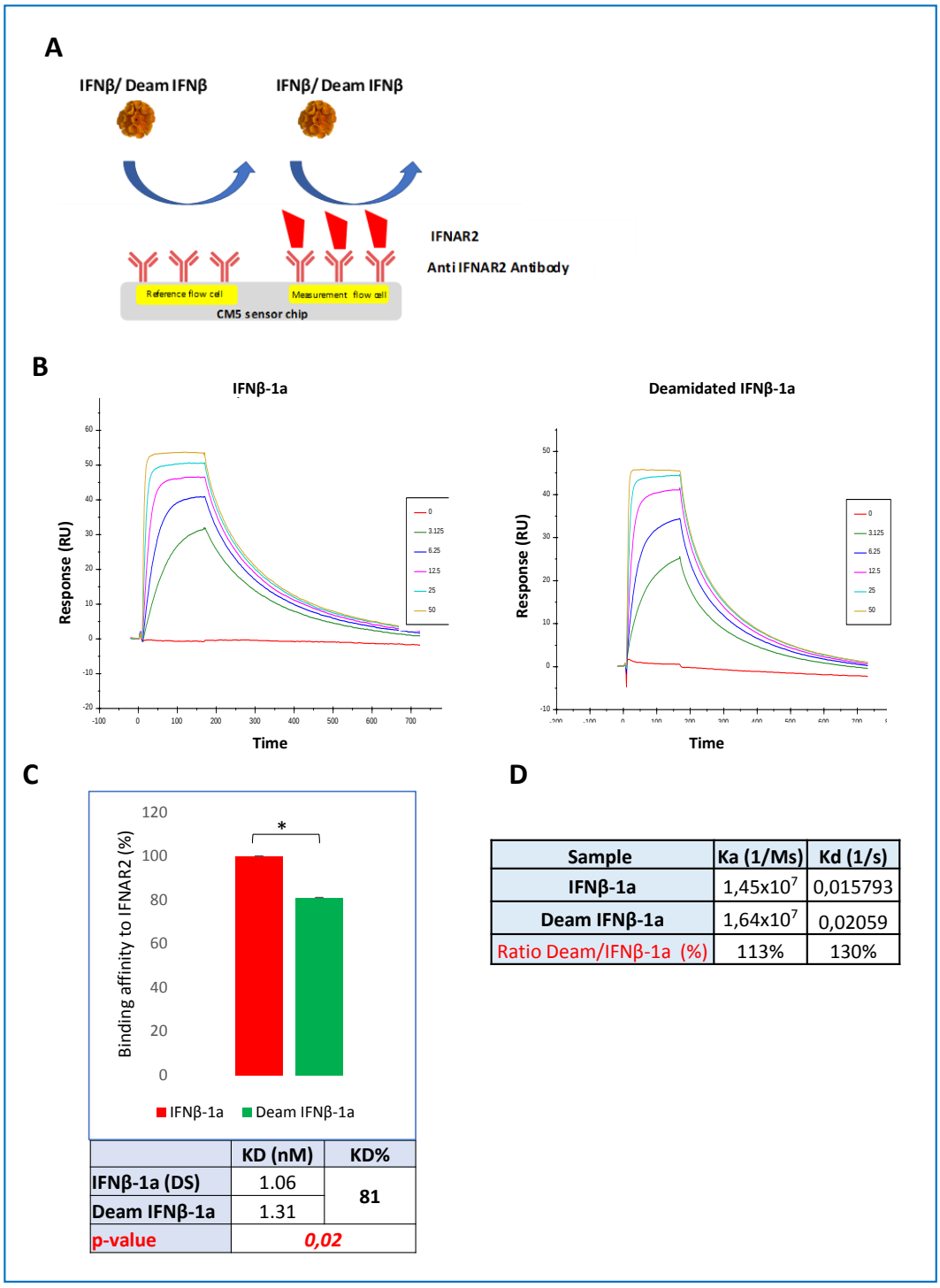

	KD (nM)	KD%
IFNβ-1a (DS)	1.06	81
Deam IFNβ-1a	1.31	
p-value	*0,02*	

Sample	Ka (1/Ms)	Kd (1/s)
IFNβ-1a	$1,45x10^7$	0,015793
Deam IFNβ-1a	$1,64x10^7$	0,02059
Ratio Deam/IFNβ-1a (%)	113%	130%

Figure 20. ***A)*** *SPR layout IFNs/IFNAR2 interaction. An anti IFNAR2 antibody was immobilized on the chip. IFNAR2 was captured on the measurement flow cell and five different IFNs concentration were flown over it. SPR signal obtained is proportional to the amount of IFNs/IFNAR2 binding.* ***B)*** *Sensorgram of IFNβ-1a (left) and its deamidated variant (right). The sensorgram was obtained by injecting five increasing concentrations of interferon variants concentrations (from 50nM to 3.125nM), in a multi cycle kinetics. Each curve of the sensorgram is characterized by an increase in the signal corresponding to the association phase and a decrease in the signal corresponding to the dissociation phase of the IFNs/IFNAR2 interaction; the red line represents the blank cycle where the buffer alone was flown over the measurement flow cell (n=3)* ***C)*** *Absolute KD and deamidated IFNβ-1a Binding affinity (%KD) versus IFNAR2 has been calculated (n=3). The relative KD (KD%) is graphically represented in the bar chart. *p <0.05 as determined by one-way ANOVA.* ***D)*** *Kinetic constant of IFNβ-1a and deamidated variant has been calculated. Differences in kinetics profile are reported as ratio of deamidated ka and kd versus IFNb-1a ones.*

4.6 BINDING AFFINITY TO IFNAR1

In order to verify the receptor affinity of the deamidated IFNβ-1a to IFNAR1, a different layout via SPR analysis was assessed. IFNAR1 was immobilized on a NTA sensor chip via His-tag capturing and the same concentration range (22, 15, 7.5, 3.75, 1.875 nM) for both interferon samples were injected over it (Figure 21A).

Despite the SPR software manages to fit both IFNβs sensorgrams and elaborates a KD result, the value of the obtained experimental Rmax, critical parameter for accurate SPR measurements, was considerably lower (~10-fold) compared to the theoretical value (data not shown). Since in SPR analysis the theoretical Rmax should be similar to the experimental one, the KD obtained from each interferon analysis could not be reliable and it was not considered to provide binding assessment. For this reason, only a qualitative analysis can be carried out.

Focusing on the samples sensorgrams, a difference in binding signal is observed. Indeed, starting from the same samples concentration range, the obtained binding to IFNAR1 is higher, in terms of RU, in the deamidated IFNβ system (Figure 21B). This difference is well described in the last concentration point and it is graphically reported in the bar chart (Figure 21B, Right).

In order to better analyze the different behavior of deamidated IFNβ-1a in receptor binding, sensorgram comparison was applied to characterized its kinetic profile compared to native IFNβ-1a.A standard deviation corridor representing IFNβ-1a (control sample) was used to compare deamidated IFNβ-1abinding data and obtain a similarity score. The results show a change in deamidated IFNβ-1a kinetic profile, especially in the association step where the deamidated sample is similar only for the ~50% to IFNβ-1a while a smaller difference in dissociation rate has been found between the interferons (Figure 21C).

The similarity score of deamidated variant was confirmed by the kinetic constants, ka and kd, obtained from this experiment. Indeed, as shown in Figure 21D, IFNβ-1a deamidation induced a higher ka and lower kd compared to its native form. However, according to the similarity score, the greatest kinetic difference occurs in association profile (153%).

This kinetic profile, characterized by a fast association rate and a slow dissociation rate, is representative of a higher affinity between ligand and analyte.

A

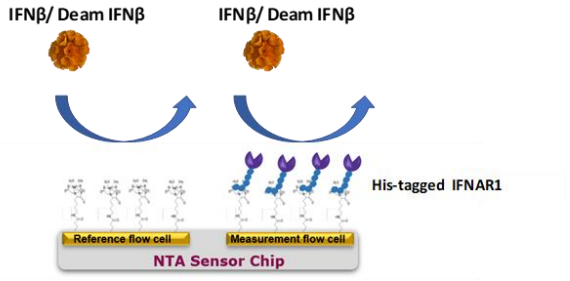

B

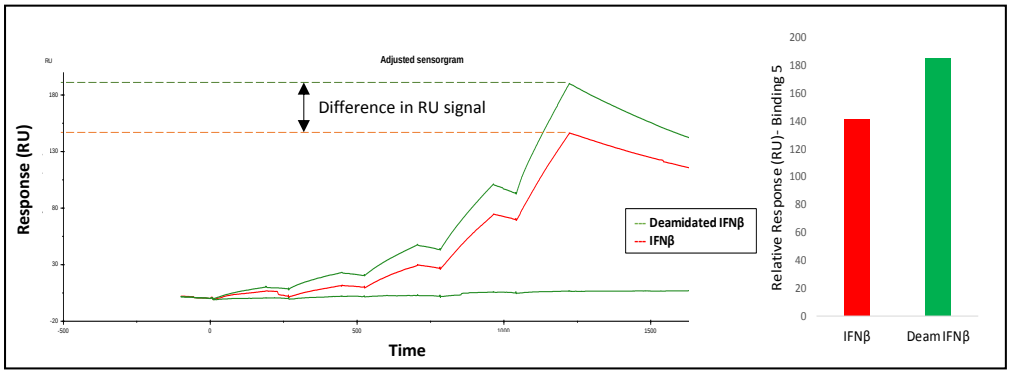

C

Deamidated IFNβ-1a Similarity Score (%)	
Association	**Dissociation**
53,47	87,85

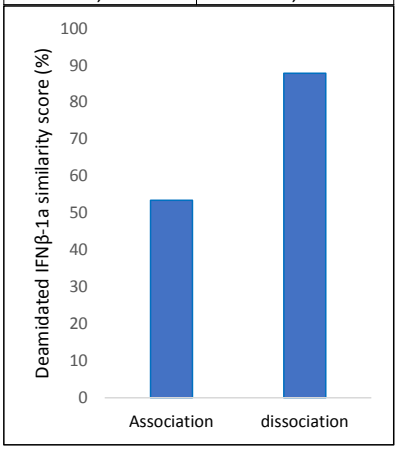

D

Sample	Ka (1/Ms)	Kd (1/s)
IFNβ	24100	0,005121
Deam IFNβ	36900	0,004247
Ratio Deam/IFNβ (%)	153	83

*Figure 21. **A)** SPR layout IFNs/IFNAR1 interaction. An His-tagged IFNAR1 was captured by NTA sensor chip in measurement flow cell. Five IFNs concentrations were flown over both flow cell. SPR signal obtained is proportional the amount of analyte/ligand binding. **B)** Representative binding affinity sensorgram of IFNß-1a (Red) and deamidated IFNß (Green). The sensorgram was obtained by injecting five increasing concentrations of interferon variants concentrations, in a single cycle kinetics. Each step of the sensorgram represents a different concentration of IFNß-1a. For each concentration, the greatest binding signal is visible in the presence of the deamidated IFNb-1a. The highest concentration tested was plotted with a bar chart to quantify the difference between IFNß-1a and deamidated variant (n=3). **C)** Deamidated IFNß-1a similarity score in association and dissociation profile and related-bar chart. The deamidated sample shows a great difference in association profile (53,47%) compared to IFNß-1a. **D)** The sensorgram was fitted by the "1:1 binding" algorithm in order to determine the association (ka) and dissociation (kd) rate constants for each sample.*

4.7 BINDING AFFINITY TO TERNARY COMPLEX

Once the different affinity of deamidated IFNβ-1a to the single receptor chains was identified, the binding to the whole ternary receptor complex was evaluated via AlphaScreen technology. In this layout, Donor beads is linked to IFNAR1 while Acceptor beads with IFNAR2. The same concentration range for both IFNβ-1a and deamidated variant was tested to evaluate the receptor binding. In presence of the IFNβ-1a variants, the two beads become a pair and when they are close, a chemiluminescent signal is generated (Figure 22A). As shown in figure 22B, the dose-response curves obtained were significantly different (p value <0,001), with a higher signal in the deamidated sample curve. Since P value is minor than 0.05, the potency cannot be calculated. For this reason, the efficacy of both interferon beta was evaluated. Efficacy is the ability of a drug to produce a maximum response. Differences in drug efficacy are evaluated by comparing the maximal response at high drug doses or concentrations (Yartsev, 2019). Deamidated sample binds the ternary receptor complex with a higher efficacy (136%) than the native form (Figure 22C). This effect does not depend on the drug dose but on the intrinsic activity of the drug intended as a different capacity to activate the drug-receptor interaction [68].

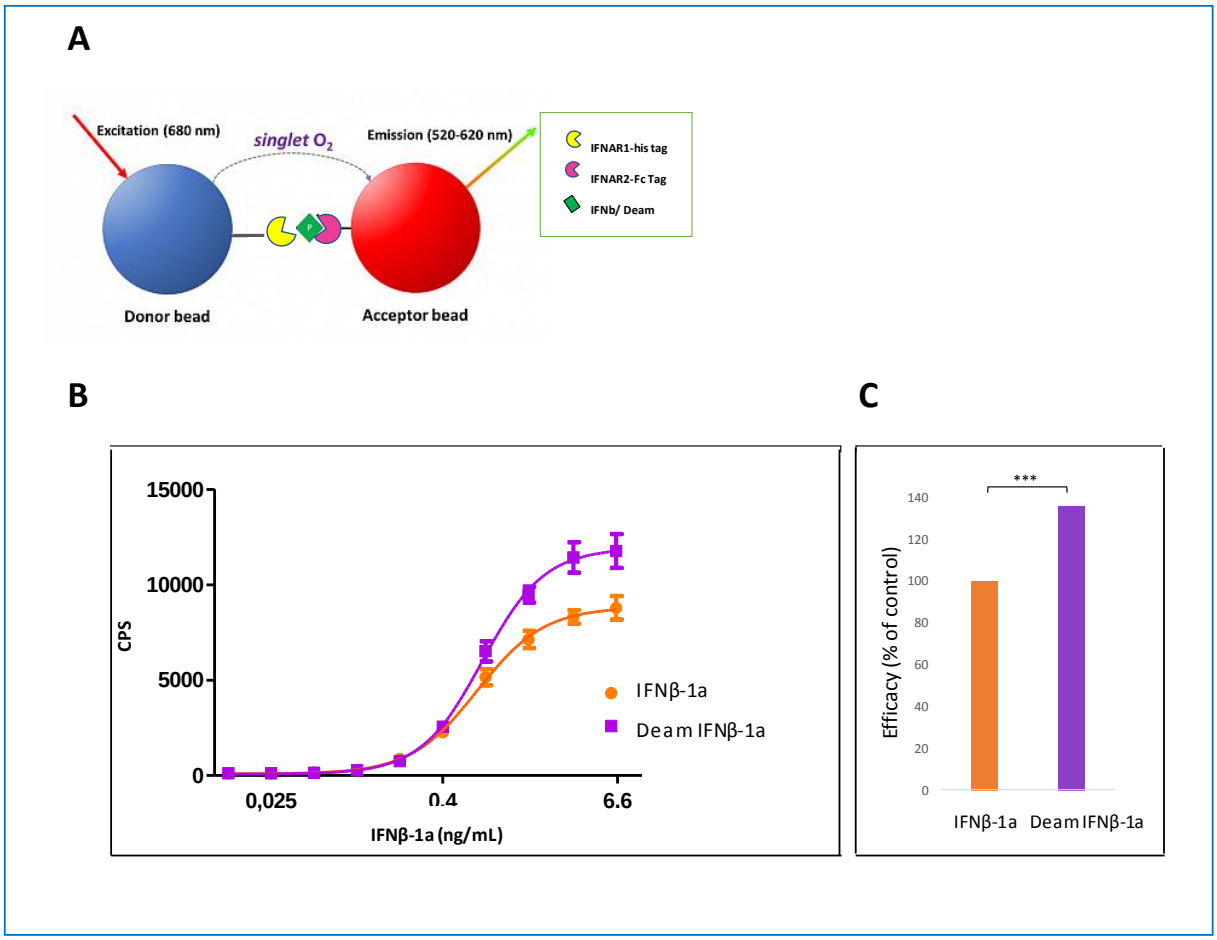

Figure 22. ***A)*** *AlphaScreen layout. Donor bead was linked to IFNAR1-his tag while Acceptor bead with IFNAR2-fc tag. When IFNβ-1a variants was added to the system, the beads move closer together generating a signal proportional to the binding between receptors and interferons.* ***B)*** *IFNβ-1a and deamidated variant were tested using the same concentration range (from 6,6 µg/mL to 0,0128 µg/mL). IFNAR1, IFNAR2 and beads mix were added to the IFNs dose-response curve and incubated for 1h. After incubation, the plate was analyzed using Envision software. Data were from three independent analytical runs.* ***C)*** *Deamidated IFNβ-1a efficacy was calculated as ratio percentage of deamidated sample to IFNβ-1a (control sample). ***P value < 0.001.*

4.8 *IN SILICO* ANALYSIS: DEAMIDATED IFNβ-1a INTERACTION PROFILE

An *in silico* analysis was carried out to further characterize the interaction profile between deamidated IFNβ-1a and its receptors chain IFNAR1 and IFNAR2. The study has been focused on structural analysis, H-Bonds network and sugar analysis. The structural analysis was performed building the three-dimensional (3D) structure of IFNAR1::IFNβ::IFNAR2 ternary complex *via* a homology modeling approach, both in native and deamidated forms (Figure 23A). A single amino acid substitution, N25D, was added in the IFNβ molecule to obtain the deamidated form (Figure 23B). Both models were N-glycosylated by adding the G2S2F glycan chain at the Asn80 position (Figure 23B). The analysis of fluctuation profiles

was performed by calculating the Root Mean Square Fluctuation (RMSF) of C-alpha atoms. This parameter has been useful to identify regions of the protein that fluctuate more and that for this were more susceptible to conformational changes. Looking at the profiles, even if the trends were conserved and comparable among two systems, some differences, especially in the N-terminal portion of IFNAR1 receptors, have been found (figure 23C). In fact, this region was more flexible in the deamidated complex than in the native one, suggesting such a conformational changed during the dynamics. Then, structural superposition of centroids of entire complexes was performed in order to visualize conformational differences between native and deamidated systems that could explain the experimentally observed divergence in receptor recognition and efficacy. However, the two centroid structures are not significantly different, especially in the receptor binding interface and a deeper investigation is needed (Figure 23D).

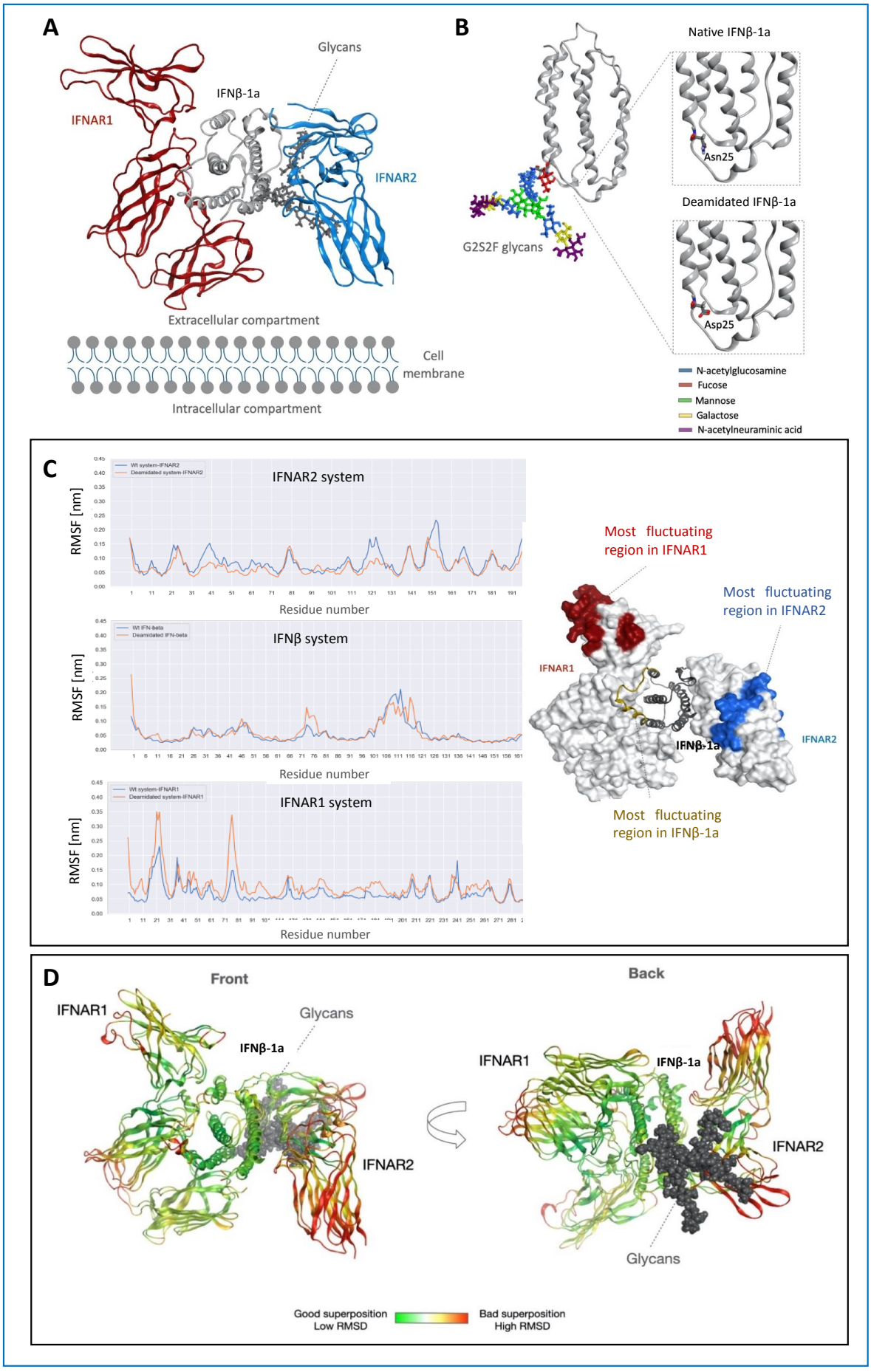
A
Glycans
IFNβ-1a
IFNAR1
IFNAR2
Extracellular compartment
Cell membrane
Intracellular compartment
B
Native IFNβ-1a
Asn25
Deamidated IFNβ-1a
Asp25
G2S2F glycans
N-acetylglucosamine
Fucose
Mannose
Galactose
N-acetylneuraminic acid
C
IFNAR2 system
IFNβ system
IFNAR1 system
RMSF [nm]
Residue number
Most fluctuating region in IFNAR1
Most fluctuating region in IFNAR2
Most fluctuating region in IFNβ-1a
IFNAR1
IFNAR2
IFNβ-1a
D
Front
Back
IFNAR1
Glycans
IFNβ-1a
IFNAR2
Good superposition
Low RMSD
Bad superposition
High RMSD

*Figure 23.**A)** 3D model of the IFNAR1::IFNβ::IFNAR2 complex. Secondary structure was rendered as colored ribbons: IFNβ was colored in grey, IFNAR1 in red and IFNAR2 in blue. Glycan atoms were rendered as dark grey sticks. The cell membrane was illustrated to facilitate the orientation of the complex. **B)** A focus on Asn/Asp25 position that is the only difference among the two complexes. Glycans were represented as sticks colored according to Symbol Nomenclature For Glycans (SNFG) system. **C)** RMSF of C-alpha atoms vs residue number of wild type (in blue) and deamidated (in orange) systems. The RMSF contribution of each protein of the complex (native in blue and deamidated in orange) was reported, highlighting some regions of major fluctuation. On the right, a structural representation of the complex in which the molecular surface of receptors was showed, with most fluctuating regions colored in red (IFNAR1) and blue (IFNAR2). IFNβ-1a variant was rendered as grey and gold (high fluctuation) ribbons. **D)**The structural superposition showed a great difference in orientation of IFNAR2, suggesting a different recognition mechanism. RMSD is an index of possible conformational changes. IFNAR1, IFNAR2 and IFNβ-1a are rendered as ribbons colored according to a RMSD gradient: in red bad superposed regions, in green good superposed ones.*

So, to support experimental results, an investigation on the hydrogen bonds (H-bonds) interaction network between IFNβ and receptors has been performed. The type and number of H-bonds was computed according to Baker-Hubbard criterion, using a threshold of 30%. This means that only bonds occurring with a frequency equal or up to 30% have been reported. Basing on this analysis, a decrease of H-bonds number among deamidated IFNβ-1a and IFNAR2 during the simulation has been observed compared to the native system (Figure 24A, top). The interaction interface between IFNβ and IFNAR1 is also quite different in the native and deamidated complexes, in terms of number and type of bonds. Only two interactions are conserved in this case (Asn86-Gln299, Arg128-Glu98), suggesting a different recognition mechanism of the IFNAR1 by the two IFNβ forms (Figure 24A, bottom). This comparison shows that some of critical residues identified by Runkel [69] are part of the network of interaction of deamidated species. In partocular, Arg71 and His131 are located in key regions for IFNAR1 recruiting. According to Runkel results, two other residues of the network of *in silico* interaction, His 93 and His 97, are in a critical region for the receptor interaction. On the opposite, most of them are non-critical by Runkel analysis: Ser119, Ther112 and Ser 118, located in the CD loop. So, according to this analysis, the N25D mutation can induce a reorientation both of IFNβ regions that are typically not involved in the interaction with IFNAR1, i.e. the CD loop, and of those considered crucial for it involving more residues in the binding to the receptor and enhancing the signaling cascade.

Since the only structural difference between the two IFNβ-1a systems was given by the N25D mutation, Asp25 interaction network in deamidated system was compared to that of Asn25 in native IFNβ-1a. As shown in Figure 24B, Asp25 in deamidated system interacts with Trp79 and not with Gly78 as in native one. The difference in H-bonds network observed for Asp25 does not impact the structural integrity of the molecule but induces a change in

glycans orientation, already visible in Figure 24B. So, an analysis of sugars behavior was performed to better investigate this aspect. In particular, the interaction network of sugars and proteins was computed, pointing out that sugars mostly interact with IFNβ-1a and IFNAR2, but never with IFNAR1(data not shown). In figure 24C sugars interacting with IFNβ-1a variants were reported, suggesting a different interaction network among the two interferon that particularly involves the Fucose (FUC) unit. In fact, Fucose, partially changes its interaction network in the deamidated form with respect to the native one, by losing the specific H-bond with Asn25, that in the deamidated IFNβ-1a was mutated in Asp (Figure 24D). The loss of this interaction probably induces a conformational change in the oligosaccharide chain that results to be differently oriented.

A

Native IFNß-1a	*IFNAR2*	*Deamidated IFNß-1a*	*IFNAR2*
Arg11	His187	Arg11	Glu190
Trp22	Asp104	Arg27	Asp9
Arg35	Thr44, Ile45, Glu50	Arg35	Ile45, Lys48, Glu50
Arg152	Glu77	Arg152	Glu77
Tyr155	Gln136		
Asn158	Asp138		
Arg165	Glu157		

Native IFNß-1a	*IFNAR1*	*Deamidated IFNß-1a*	*IFNAR1*
Asn86	Gln299	Asn86	Gln299
Glu103	Arg268	Arg71	Asp152
Asp110	Trp210	His93	Asp325
Lys123	Thr208	His97	Asp325
Arg124	Glu98	Thr112	Leu207
Gly127	Asn95	Ser118	Thr208
Arg128	Glu98	Arg128	Glu98
		Arg124	Glu98, Tyr97
		Ser119	Arg124
		His131	Leu94

B

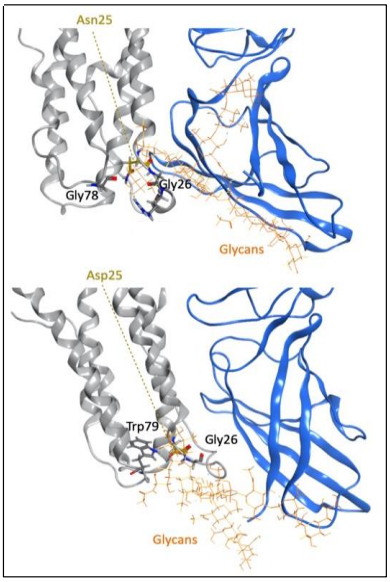

C

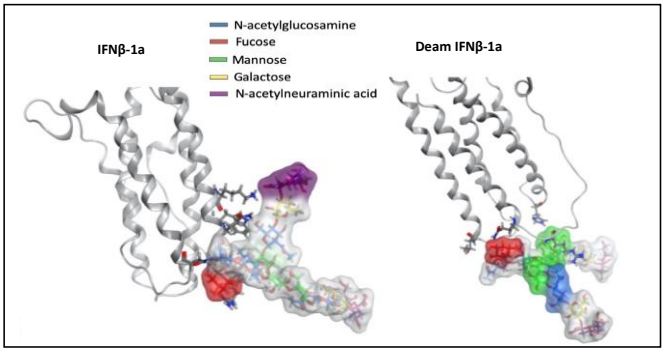

D

G2S2F chain	IFNβ-1a
FUC2	Asn25, GLy26, Asn80
NEU12	Lys19, Trp22, Gln23
MAN6	Arg27

G2S2F chain	Deam IFNβ-1a
FUC2	Gln23, Thr82
NEU12	Arg27
MAN6	His140

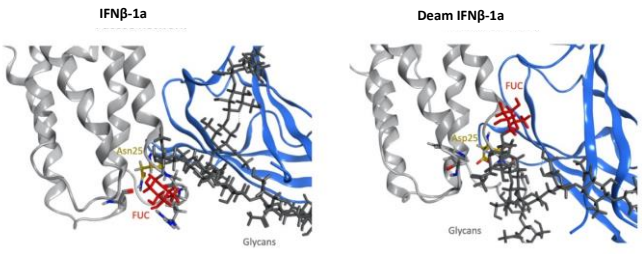

*Figure 24. **A)** On the top, H-bond interactions between IFNß-1a variants and IFNAR2 has been reported.. On the bottom, H-bond interactions between IFNß-1a variants and IFNAR1 has been reported. The interactions common to both systems were colored. **B)** Asn/Asp25 interaction network; IFNß-1a variants were represented as grey, IFNAR2 as blue ribbons, glycans were rendered as orange sticks. IFNAR1 was not shown in this picture. **C)** 3D model of sugars involved in the interaction with IFNß-1a variants were colored according to SNFG system and represented as molecular surface. **D)** The sugar interaction network highlights that in native system, FUC2 interacts with Asn25 while this interaction is lost in the deamidated IFNß-1a, upon the mutation and the fucose changed its orientation. IFNß-1a variant has been represented as grey ribbons, sugars as grey sticks and fucose as red sticks.*

An analysis of dihedral angles was performed for glycans to estimate their conformational variability. By this analysis a different ability to explore the conformational space was recognized for NAG1-FUC2 and for MAN5-NAG7 couples among systems. In particular, it

has been observed that NAG1-FUC2 dihedral showed a higher mobility in the deamidated system with respect to the native one, thus confirming that the loss of the interaction with Asn25 induced a change in the conformation of this sugar and of all the chain (Figure 25A). The different sugars orientation in the deamidated system could affect the interaction with IFNAR2 chain. H-bonds between sugar and IFNAR2 were computed using the Baker-Hubbard criterion and considering as a threshold a frequency equal or up to 5%. In deamidated system, the interaction between IFNAR2 and sugars was characterized by an extremely reduced number of hydrogen bonds compared to the native form (figure 25B). In particular, already published works, proposed that Neu can play a role in stabilizing the IFNβ::IFNAR2 complex [70] and its interaction with IFNAR2 are reduced in deamidated system.

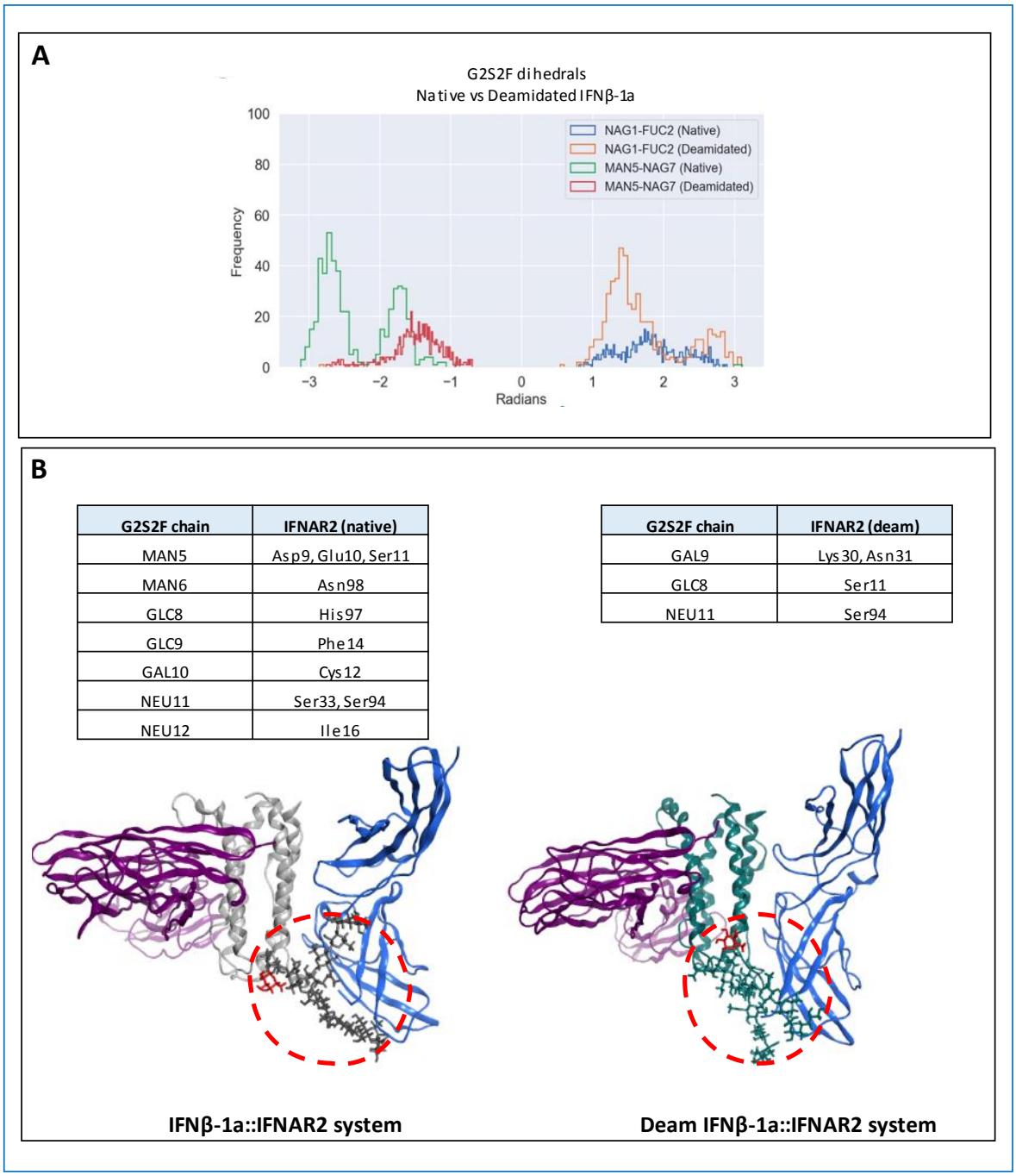

G2S2F chain	IFNAR2 (native)
MAN5	Asp9, Glu10, Ser11
MAN6	Asn98
GLC8	His97
GLC9	Phe14
GAL10	Cys12
NEU11	Ser33, Ser94
NEU12	Ile16

G2S2F chain	IFNAR2 (deam)
GAL9	Lys30, Asn31
GLC8	Ser11
NEU11	Ser94

Figure 25. ***A)*** *Conformational changes in sugars NAG1-FUC2 and MAN5-NAG7.* ***B)*** *In the table, the H-bonds network between sugar and IFNAR2 observed in the native and deamidated system has been reported. A structural representation of sugar and IFNAR2 complex in native and deamidated forms is showed. IFNAR1 was represented in violet, IFNAR2 in blue. IFNb1-a was colored in light grey while its deamidated variant in green. Sugars were represented inside the red circle as dark grey in native system and green in deamidated one. Fucose has been colored in red.*

4.9 MAPK and NFKB SIGNALING PATHWAY EVALUATION AND PROTEOMIC ANALYSIS

In order to identify other MoAs of the deamidated IFNβ-1a, the role of this molecule in other signaling pathway, such as MAPK and NF-kB, was assessed.

To evaluate if deamidated IFNβ-1a could affect differently the MAPK compared to its native form, the phosphorylation of ERK, JNK and P38 was evaluated. For this purpose, A549 were treated with 50ng/mL of deamidated IFNβ-1a and its native form at the indicated time points (Figure 26).

As shown in Figure 26 B-C, pP38 and pJNK were not activated by the Interferons treatment. Contrarily, ERK phosphorylation was differently influenced by treatment anddrug exposure time (figure 26A). Under short-term IFNs exposure, ERK phosphorylation raised up to 15 minutes, while at 60min it returned to the basal state. However, both interferons induced the same ERK activation trend and no differences have been found between the two treatments.

Next, NF-kB pathway was evaluated. To assess if deamidated IFNβ-1a affected NF-kB activity, A549 cell line were treated with 20ng/mL of each interferon variant for 30 minutes. As shown in Figure 26D, both interferons lead to a slight reduction of NF-kB phosphorylation and no significant differences has been detected between the two IFNβ-1a variants.

Based on these results, a proteomic analysis was performed to evaluate a biological effect of deamidated variant to additional proteins and signaling. With this aim, A549 were treated for 24h with 1ng/mL of deamidated IFNβ-1a and its native variant. Untreated cells were used as control to evaluate changes in protein expression induced by the treatments. Following exposure to interferon variants, the proteins released from the cells in colture media have been determined and reported in Figure 26E. Both IFNβ-1a and deamidated variant induce the release of pro and anti-inflammatory cytokines, such as IL-6, IL-12 and type I IFN. The only difference observed in the two systems was the release of IL-8 which occurs following the exposure of IFNB-1a but not with deamidated form indicating a different biological response between the two variants.

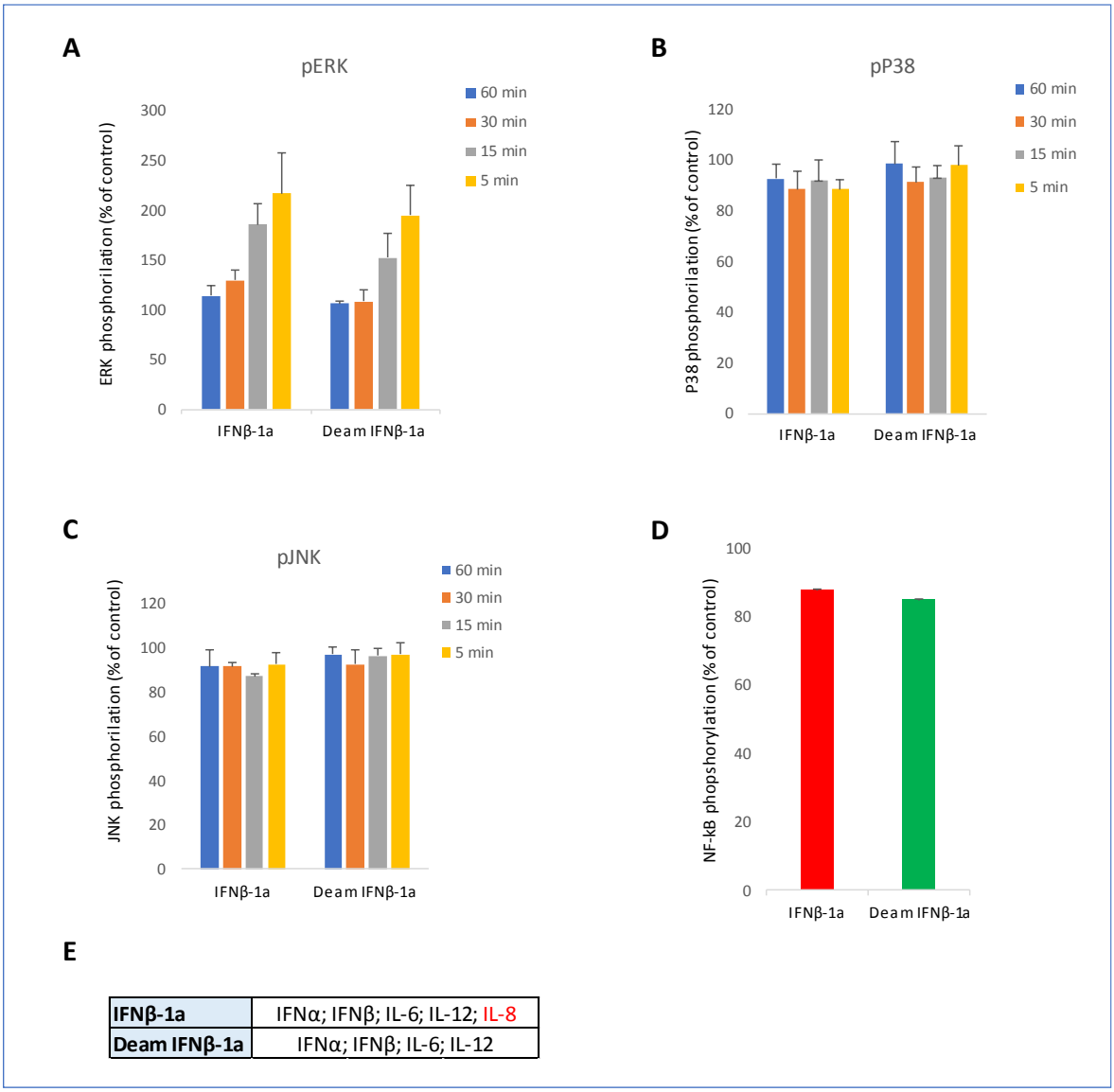

IFNβ-1a	IFNα; IFNβ; IL-6; IL-12; IL-8
Deam IFNβ-1a	IFNα; IFNβ; IL-6; IL-12

*Figure 26. **A-B-C)** MAPK phosphorylation under IFNβ-1a variants treatment. A549 cell line were exposed to both IFNβ variants treatment at different time point (from 5 min to 60min). The phosphorylation of ERK **(A)** P38 **(B)** and JNK **(C)** of treated cells was analyzed and normalized on the untreated (CTRL) (n=3). **D)** IFNs effect on NF-kB phosphorylation. A549 cell line were exposed at short term IFNβ-1a variants treatment (30min). After treatment, the phosphorylation was analyzed for each condition and the obtained results were normalized on the untreated cells (CTRL) (n=2). **E)** Protein expression induced by IFNβ-1a variants treatment compared to the CTRL. IL-8 expression is induced only under native IFNb-1a treatment (red).*

5 DISCUSSION

Deamidation is a common post- translational modification of L- asparagine (Asn) residues leading to an Asn to Asp / IsoAsp mutation. Usually, deamidation is undesirable in biopharmaceuticals due to its possible effect on protein structure, function, stability and immunogenicity. However, the impact of deamidation on drugs may not necessarily represent negative changes in the function and quality of the molecule of interest [71]. Indeed, previous study reported an increased biological activity of IFNβ-1a after artificial deamidation [33]. As reported by Mastrangeli *et al*., the artificial deamidation treatment leads to an almost fully deamidated IFNβ-1a form without affecting other properties, like glycoforms distribution, methionine oxidation and protein aggregation. Due to the continual require by the Health Authorities to identify and manufacture more potent biologically active agents, this work has been focused on the deamidated form of the IFNβ-1a for its therapeutic potential. The main goal was to discover the mechanism underlying its higher biological response.

First, the development of new cell-based assays was needed to confirm the biological activity of the deamidated cytokine. The biological activity of this molecule was already assessed by applying specific bioassays that are part of the Rebif characterization analytical panel[33]. However, these bioassays were developed many years ago and they were characterized by relevant method variability that could affect the samples comparability results. The development and qualification of dedicated methods with higher precision and accuracy allows to ensure a reliable result and, at the same time, can be proposed for an update of the analytical panel of Rebif, as suggested by the regulatory authorities in the frame of continuous improvement framework. In this context, two new cell-based methods mimicking the immunomodulatory and antiviral MoA, have been developed to overcome the limits of the current methods and have more precise and performing procedures to test the molecule of interest. The immunomodulatory assay, able to measure the MHC I expression induced by IFNβ-1a treatment, has been developed starting from the optimization of the previous immunomodulatory assay. Differently, antiviral assay, able to measure the antiviral activity of deamidated IFNβ-1a, has been developed from scratch using a reporter gene system. RGA is commonly used for its simplicity, high specificity and sensitivity and it is accepted by regulatory agencies if they reflect the mode of action of the drug. Several parameters have been tested in both methods to obtain the best-dose response curve and meet

all the acceptance criteria reported in ICH guidelines. Immunomodulatory assay and RGA has been improved in terms of precision and accuracy and the obtained results demonstrate the assays suitability for characterization and comparability purpose.

Once both methods have been qualified, they were used to test accurately the potency of deamidated IFNβ-1a.

The obtained results show a 2-fold higher antiviral and immunomodulatory activity of deamidated variant compared to the native IFNβ-1a. These data, confirming the previous study, kicked off the investigation of the mechanism underlying this effect.

Logically, the attention was initially only focused on the IFNβ-1a canonical pathway. It is well established that IFNβ-1a exerts its biological response via the JAK-STAT signaling pathway. However, some studies suggest that interferon beta could activate a non-conventional signal transduction [17,72]. For this reason, the activity of the canonical IFNβ-1a pathway has been evaluated to assess the involvement of the conventional signaling in the observed cellular responses. In particular, STAT1 phosphorylation and ISGs expression has been evaluated. STAT1, the primary transcription factor activated by IFNβ-1a, is considered the more sensitive and reliable biomarker than other pathway-specific activated STATs [38]. The obtained results showed the ability of Deamidated IFNβ-1a treatment to induces a significant increase in STAT1 phosphorylation compared to its native form. The higher signaling activity due to IFNβ-1a deamidation is translated in a consequent increase in target gene expression. Indeed, HLA-C and MX1 genes were found 2-fold up-regulated after 24h of deamidated interferon treatment in respect with the native form. This result further confirms the higher response induced by deamidated IFNβ-1a. Moreover, both gene expression and biological activity show the same trend (2-fold increase) when exposed to the deamidated variant, highlighting the close correlation between the two effects. Once the involvement of the canonical signaling pathway has been established, the attention has been focused on receptor binding. Several hypotheses have been proposed to explain the increasing biological activity of deamidated IFNβ-1a. Mastrangeli and colleagues, considering the three-dimensional (3D) orientation of Asn25, suggested that its deamidation can induce an increase of electrostatic interactions mediated by Asp25 influencing the receptor binding affinity [33]. Since the receptor-ligand affinity is important for regulating the signal strength through the membrane and the subsequent signaling [73], an increase in binding affinity to IFNAR has been hypothesized as a cause of the increased biological activity of deamidated IFNβ-1a. Since the biological activity of biopharmaceutical is determined by its

protein conformation which can be affected by post-translational modifications (PTM) [74], deamidation process could induce an IFNβ-1a conformational change resulting in a higher receptor affinity. Based on this hypothesis, differences in binding affinity of deamidated IFNβ-1a in comparison with its native form has been assessed via several approaches. First, the attention has been focused on the high affinity IFNAR2 receptor chain. Surprisingly, deamidated variant showed a faster dissociation rate leading to a decrease in binding affinity (~20%) versus this receptor chain. These results were not expected and they did not clarify the higher biological activity of deamidated IFNβ-1a. For this reason, a change in affinity of deamidated IFNβ-1a to IFNAR1 has been considered as cause of this phenomenon and the related binding has been assessed. Comparing the binding of each IFNβ-1a variants to IFNAR1, the two system demonstrate a different behavior. The obtained sensorgrams show a difference in terms of signal (RU) and kinetic profiles, as confirmed by the similarity score. In particular, deamidated samples is characterized by a slow dissociation and a fast association rate leading to a higher affinity between ligand and analyte. The reduced binding affinity to IFNAR2 in the deamidated system is counterbalanced by an increase in affinity to IFNAR1. To assess if the different affinity of deamidated variant to the single receptor chain could affect the binding to the whole receptor complex, the binding efficacy of each interferon variant to IFNAR has been tested. As expected, deamidation leads to a higher binding efficacy (136%) to the ternary complex compared to the native IFNβ-1a. Taking in account these results, deamidation process induces an increase in IFNAR receptor binding thanks to the greater affinity towards IFNAR1. Experimental results were further confirmed and integrated with *in silico* data useful to investigate the dynamics of IFNAR1::IFNβ::IFNAR2 ternary complex both in native and in deamidated form. According to these data, the presence of Asp instead of Asn (N25D mutation) in IFNβ-1a induces a change in the interaction network in that region provoking a change also in G2S2F glycans orientation that is transposed in a different recognition mechanism of IFNAR2. This was suggested by dihedrals angles distribution analysis demonstrating that in the deamidated form the glycan chain rotates around the fucose changing its conformation and losing interactions with the IFNAR2. In particular, in the native system, fucose is locked in a specific state by the interaction with Asn25 that allows a rotation of the G2S2F glycans chain that is more prone to interact with IFNAR2. On the other hand, in the deamidated complex, the loss of some interactions of the fucose in the Asp25 region, makes sugars able to adopt an extended conformation less prone to interact with IFNAR2. Indeed, looking in detail at

the interactions reported by the H-bonds analysis between sugars in deamidated IFNβ-1a and IFNAR2, some of them have been lost during the dynamics, suggesting that the different sugars orientation could be responsible for a reduction of binding affinity between deamidated IFNβ-1a and IFNAR2. In addition, according to the H-bonds analysis, in the case of IFNAR1 a difference in the residues involved in the recognition was highlighted, suggesting that a conformational change due to the mutation, even if slight, can induce the involvement of such residues in the IFNAR1 binding. Indeed, the most of identified residues have been demonstrated to be critical for the interaction by mutagenesis studies [69] strongly supporting and suggesting that the N25D mutation can facilitate the exposure towards to the receptor of more key residues that interact with it and enforce the biological response. Together to this, also other residues considered not typically involved in the interaction were found to bind the receptor, suggesting that an involvement of regions not commonly considered critical may be possible.

So, probably the loss of interactions with IFNAR2 promotes the interaction with IFNAR1 in a not conventional way, that however can positively impact the complex formation and the biological activity of the product. Taken together all the *in silico* results confirm the data obtained by SPR analysis and give a structural explanation of the reduced affinity of the deamidated IFNβ-1a for IFNAR2 and a higher affinity to IFNAR1. Given the strong correlation between receptor binding and biological activity, the increased deamidated IFNβ-1a receptor affinity can be considered the mechanism underlying the higher biological activity of this molecule.

In addition, with the aim to possibly explore other therapeutic areas and foster the product knowledge about the yet unknown potential of the drug, the scouting of new possible IFNβ-1a MoAs has been carried out. MAPK and NF-kB signalling pathway has been considered related interferon pathways and their activity has been evaluated under interferon treatment. However, the results obtained do not show any additional effect on these pathways except in ERK phosphorylation. Both interferon variants induce an increase in ERK activity after 5 minutes of treatment. Although a reduction in MAPK was expected given the antiproliferative activity of IFNβ-1a, the fast up-regulation of MAPK under interferon exposure is reported to be correlated with the antiviral activity [15]. However, the two drugs produce the same effect on ERK phosphorylation and in general on MAPK and NF-kB pathways. Therefore both signaling pathways cannot be considered involved in an additional MoAs of deamidated IFNβ-1a. In order to extend the attention to further proteins potentially

involved in further MoAs of the deamidate variant, a proteomic analysis has been carried out. Preliminary results show pro and anti inflammatory cytokine expression following treatment, bringing the focus to IL-8. Indeed, in contrast with native IFNβ-1a, deamidated variant did not induce a release of IL-8.Interleukin-8 has been associated to tumor metastasis. Indeed, this cytokine actsas a potent angiogenic factor in several cancers including Non Small Cell Lung Cancer (NSCLC)[77 78]. Elevated IL-8 is correlated with tumour progression and poor survival in NSCLC[78–80]. The connection between IFNβ and IL-8 has not been much studied in lung cancer. These preliminary results indicate a possible different mechanism of deamidated samples and open new perspective for more in-depth studies.

6 CONCLUSION

In conclusion, the mechanism underlying the higher MoA of deamidated interferon has been discovered in this work. Deamidation leads to a change in receptor interaction network, increasing IFNAR1 receptor binding affinity. Since this receptor chain is essential to activate IFNβ-1a signaling pathway, the change in receptor affinity can be considered the key of the observed deamidated IFNβ-1a biological behavior. Despite the binding efficacy of deamidated IFNβ-1a/IFNAR is not very high compared to the native system, it is sufficient to lead to an increase in JAK-STAT signaling pathway activity inducing, via signaling amplification, a 2-fold higher gene expression and consequent biological response.

This work has highlighted new aspects of Rebif biological behavior and opens new perspectives for considering the deamidated variant as a new drug. Increasing the scientific knowledge of a molecule is critical to better understand the biological behavior of the drug of interest and for improving the life quality of patients. Thanks to its greater biological activity, deamidated IFNβ-1a could be used to improve current therapies or introduce a synergistic agent in oncology/immunoncology (combination therapy). Indeed, considering its pharmaceutical potential, a drug repositioning of the molecule of interest can be considered. Although Rebif was born for the treatment of multiple sclerosis, interferons have been found to have several effects against different types of tumor even in advanced stage, including lung cancer. In particular, evidence of radiosensitization by IFNβ has been reported [81]. Moreover, given the role of IL-8 in lung cancer and hepatitis B pathogenesis, deamidated IFNβ-1a could be considered a possible treatment for the reduction of tumor progression and angiogenesis in lung cancer and a more powerful antiviral drug to fight hepatitis without overloading IL-8, a biological response that cannot be fully achieved with native interferon. More in-depth studies and future *in vivo* analysis will be needed to confirm the therapeutical potential of deamidated interferon and its efficacy against other malignancies.

7 REFERENCES

1. Kalliolias, G. D. & Ivashkiv, L. B. Overview of the biology of type I interferons. *Arthritis Research and Therapy* vol. 12 S1 (2010).

2. Wang, H. H. ; Z. K. Overview of Interferon: Characteristics, signaling and anti-cancer effect. *Arch. Biotechnol. Biomed.* **1**, 001–016 (2017).

3. Schneider, W. M., Chevillotte, M. D. & Rice, C. M. Interferon-stimulated genes: A complex web of host defenses. *Annual Review of Immunology* vol. 32 513–545 (2014).

4. Levy, D. E. Whence interferon? Variety in the production of interferon in response to viral infection. *Journal of Experimental Medicine* vol. 195 f15 (2002).

5. Meager, A. The interferons: Past, present and future. *Dig. Liver Dis. Suppl.* **3**, 3–8 (2009).

6. Presnell, S. R. & Cohen, F. E. Topological distribution of four-alpha-helix bundles. *Proc. Natl. Acad. Sci. U. S. A.* **86**, 6592–6596 (1989).

7. Karpusas, M., Whitty, A., Runkel, L. & Hochman, P. The structure of human interferon-β: Implications for activity. *Cellular and Molecular Life Sciences* vol. 54 1203–1216 (1998).

8. Karpusas, M. *et al.* The crystal structure of human interferon β at 2.2-Å resolution. *Proc. Natl. Acad. Sci. U. S. A.* **94**, 11813–11818 (1997).

9. CS, R., CS, H., AP, A., TE, S. & RM, R. Expression of interferon receptor subunits, IFNAR1 and IFNAR2, in the ovine uterus. *Biol. Reprod.* **67**, (2002).

10. De Weerd, N. A., Samarajiwa, S. A. & Hertzog, P. J. Type I interferon receptors: Biochemistry and biological functions. *Journal of Biological Chemistry* vol. 282 20053–20057 (2007).

11. Piehler, J., Thomas, C., Christopher Garcia, K. & Schreiber, G. Structural and dynamic determinants of type I interferon receptor assembly and their functional interpretation. *Immunol. Rev.* **250**, 317–334 (2012).

12. Thomas, C. *et al.* Structural linkage between ligand discrimination and receptor activation by Type i interferons. *Cell* **146**, 621–632 (2011).

13. Stanifer, M. L., Pervolaraki, K. & Boulant, S. Differential regulation of type I and type III interferon signaling. *International Journal of Molecular Sciences* vol. 20 (2019).

14. Ivashkiv, L. B. & Donlin, L. T. Regulation of type i interferon responses. *Nature Reviews Immunology* vol. 14 36–49 (2014).

15. Zhao, L. J., Hua, X., He, S. F., Ren, H. & Qi, Z. T. Interferon alpha regulates MAPK and STAT1 pathways in human hepatoma cells. *Virol. J.* **8**, 157 (2011).

16. Romerio, F., Riva, A. & Zella, D. Interferon-α2b reduces phosphorylation and activity of MEK and ERK through a Ras/Raf-independent mechanism. *Br. J. Cancer* **83**, 532–538 (2000).

17. Du, Z. *et al.* Non-conventional signal transduction by type I interferons: The NF-κB pathway. *J. Cell. Biochem.* **102**, 1087–1094 (2007).

18. Pfeffer, L. M. *et al.* Role of nuclear factor-κB in the antiviral action of interferon and interferon-regulated gene expression. *J. Biol. Chem.* **279**, 31304–31311 (2004).

19. Manna, S. K., Mukhopadhyay, A. & Aggarwal, B. B. IFN-α Suppresses Activation of Nuclear Transcription Factors NF-κB and Activator Protein 1 and Potentiates TNF-Induced Apoptosis. *J. Immunol.* **165**, 4927–4934 (2000).

20. Pfeffer, L. M. The role of nuclear factor κb in the interferon response. *Journal of Interferon and Cytokine Research* vol. 31 553–559 (2011).

21. Meager, A. Biological assays for interferons. *Journal of Immunological Methods* vol. 261 21–36 (2002).

22. Apelbaum, A., Yarden, G., Warszawski, S., Harari, D. & Schreiber, G. Type I Interferons Induce Apoptosis by Balancing cFLIP and Caspase-8 Independent of Death Ligands. *Mol. Cell. Biol.* **33**, 800–814 (2013).

23. Kopitar-Jerala, N. The role of interferons in inflammation and inflammasome

activation. *Frontiers in Immunology* vol. 8 873 (2017).

24. Madsen, C. The innovative development in interferon beta treatments of relapsing-remitting multiple sclerosis. *Brain and Behavior* vol. 7 (2017).

25. Sanford, M. *et al.* Subcutaneous recombinant interferon-β-1a (Rebif®): A review of its use in the treatment of relapsing multiple sclerosis. *Drugs* vol. 71 1865–1891 (2011).

26. Lamanna, W. C. *et al.* Maintaining consistent quality and clinical performance of biopharmaceuticals. *Expert Opinion on Biological Therapy* vol. 18 369–379 (2018).

27. Mastrangeli, R. *et al.* In vitro biological characterization of IFN-β-1a major glycoforms. *Glycobiology* **25**, 21–29 (2015).

28. Liu, L. Antibody glycosylation and its impact on the pharmacokinetics and pharmacodynamics of monoclonal antibodies and Fc-fusion proteins. *Journal of Pharmaceutical Sciences* vol. 104 1866–1884 (2015).

29. Conradts, H. S. *et al.* Structure of the Carbohydrate Moiety of Human Interferon+ Secreted by a Recombinant Chinese Hamster Ovary Cell Line. *J. Biol. Chem.* **262**, 14600–14605 (1987).

30. Souphatta Sasorith, M. C. and M.-P. L. Immunoglobulin (IG) or antibody glycosylation. (2020).

31. Manfredonia, F. *et al.* Review of the clinical evidence for interferon β la (Rebif®) in the treatment of multiple sclerosis. *Neuropsychiatric Disease and Treatment* vol. 4 321–336 (2008).

32. Dhib-Jalbut, S. & Marks, S. Interferon-β mechanisms of action in multiple sclerosis. *Neurology* **74**, S17–S24 (2010).

33. Mastrangeli, R. *et al.* Biological Functions of Interferon β-1a Are Enhanced by Deamidation. *J. Interf. Cytokine Res.* **36**, 534–541 (2016).

34. Robinson, A. B. Molecular clocks, molecular profiles, and optimum diets: Three approaches to the problem of aging. *Mech. Ageing Dev.* **9**, 225–236 (1979).

35. Glen Teshima. Deamidation of Proteins and Peptides: Monograph 0001. https://www.ionsource.com/Card/Deamidation/mono0001.htm.

36. Liu, S., Moulton, K. R., Auclair, J. R. & Zhou, Z. S. Mildly acidic conditions eliminate deamidation artifact during proteolysis: digestion with endoprotease Glu-C at pH 4.5. *Amino Acids* **48**, 1059–1067 (2016).

37. Robinson, N. E. Protein deamidation. *Proc. Natl. Acad. Sci. U. S. A.* **99**, 5283–5288 (2002).

38. Lee, S. *et al.* A Glycoengineered Interferon-β Mutein (R27T) Generates Prolonged Signaling by an Altered Receptor-Binding Kinetics. *Front. Pharmacol.* **9**, 1568 (2019).

39. White, J. R. *et al.* Best practices in bioassay development to support registration of biopharmaceuticals. *Biotechniques* **67**, 126–137 (2019).

40. Shi Jing and McKee Marian. Building a Robuts Bioassay for Product PotencyBioProcess International. https://bioprocessintl.com/analytical/product-characterization/building-a-robust-bioassay-for-product-potency-measurement/ (2015).

41. Bravery, C. A. *et al.* Potency assay development for cellular therapy products: An ISCT* review of the requirements and experiences in the industry. *Cytotherapy* vol. 15 9-19.e9 (2013).

42. ICH (Q5E). ICH Q5E Biotechnological/biological products subject to changes in their manufacturing process: comparability of biotechnological/biological products | European Medicines Agency. https://www.ema.europa.eu/en/ich-q5e-biotechnologicalbiological-products-subject-changes-their-manufacturing-process.

43. USP<1032>. USP 1032. **66**, 37–39.

44. ICH Q6B. *ICH Topic Q 6 B Specifications: Test Procedures and Acceptance Criteria for Biotechnological/Biological Products Step 5 NOTE FOR GUIDANCE ON SPECIFICATIONS: TEST PROCEDURES AND ACCEPTANCE CRITERIA FOR BIOTECHNOLOGICAL/BIOLOGICAL PRODUCTS*. http://www.emea.eu.int

(1999).

45. Development & Approval Process | Drugs | FDA. https://www.fda.gov/drugs/development-approval-process-drugs.

46. Umscheid, C. A., Margolis, D. J. & Grossman, C. E. Key concepts of clinical trials: A narrative review. *Postgraduate Medicine* vol. 123 194–204 (2011).

47. ICH Q8(R2). ICH Q8 (R2) Pharmaceutical development | European Medicines Agency. https://www.ema.europa.eu/en/ich-q8-r2-pharmaceutical-development.

48. Medicines Agency, E. *Committee for Human Medicinal Products ICH guideline Q10 on pharmaceutical quality system Step 5 Transmission to CHMP Date for coming into effect*. www.ema.europa.eu/contact (2015).

49. ICH Q9. *Committee for Human Medicinal Products ICH guideline Q9 on quality risk management*. www.ema.europa.eu/contact (2015).

50. Wang, X., An, Z., Luo, W., Xia, N. & Zhao, Q. Molecular and functional analysis of monoclonal antibodies in support of biologics development. *Protein and Cell* vol. 9 74–85 (2018).

51. Vulto, A. G. & Jaquez, O. A. The process defines the product: what really matters in biosimilar design and production? *Rheumatology (Oxford, England)* vol. 56 iv14–iv29 (2017).

52. Eon-Duval, A., Broly, H. & Gleixner, R. Quality attributes of recombinant therapeutic proteins: An assessment of impact on safety and efficacy as part of a quality by design development approach. *Biotechnol. Prog.* **28**, 608–622 (2012).

53. USP <1034>. Analysis of Biological Assays. https://www.drugfuture.com/Pharmacopoeia/usp35/PDF/5186-5201 %5B1034%5D Analysis of Biological Assays.pdf.

54. Thomas A. Little, P. Essentials in Bioassay Design and Relative Potency Determination | BioPharm International. https://www.biopharminternational.com/view/essentials-bioassay-design-and-relative-potency-determination (2016).

55. Camacho-Sandoval, R. *et al.* Development and validation of a bioassay to evaluate binding of adalimumab to cell membrane-anchored TNFα using flow cytometry detection. *J. Pharm. Biomed. Anal.* **155**, 235–240 (2018).

56. ICH Q2(R1). *Validation of Analytical Procedures: Text and Methodology*. https://www.ema.europa.eu/en/documents/scientific-guideline/ich-q-2-r1-validation-analytical-procedures-text-methodology-step-5_en.pdf (1995).

57. General Chapters: <1225> VALIDATION OF COMPENDIAL METHODS. http://www.uspbpep.com/usp29/v29240/usp29nf24s0_c1225.html.

58. Chemical Computing Group ULC. Molecular Operating Environment (MOE). https://www.chemcomp.com/Research-Citing_MOE.htm (2019).

59. Labute, P. The generalized born/volume integral implicit solvent model: Estimation of the free energy of hydration using London dispersion instead of atomic surface area. *J. Comput. Chem.* **29**, 1693–1698 (2008).

60. Case D.A. et al. *AMBER10*. (2008).

61. Barker, J. A. & Watts, R. O. Monte carlo studies of the dielectric properties of water-like models. *Mol. Phys.* **26**, 789–792 (1973).

62. Watts, R. O. Monte carlo studies of liquid water. *Mol. Phys.* **28**, 1069–1083 (1974).

63. Phillips, J. C. *et al.* Scalable molecular dynamics on CPU and GPU architectures with NAMD. *J. Chem. Phys.* **153**, 044130 (2020).

64. McGibbon, R. T. *et al.* MDTraj: A Modern Open Library for the Analysis of Molecular Dynamics Trajectories. *Biophys. J.* **109**, 1528–1532 (2015).

65. (No Title). http://tools.thermofisher.com/content/sfs/brochures/TR0049-Acetone-precipitation.pdf.

66. Amodio, G. *et al.* Proteomic signatures in thapsigargin-treated hepatoma cells. *Chem. Res. Toxicol.* **24**, 1215–1222 (2011).

67. UniProt. https://www.uniprot.org/.

68. Ariens, E. J. Intrinsic activity: partial agonists and partial antagonists - PubMed. https://pubmed.ncbi.nlm.nih.gov/6188923/.

69. Runkel, L. *et al.* Systematic mutational mapping of sites on human interferon-β-1a that are important for receptor binding and functional activity. *Biochemistry* **39**, 2538–2551 (2000).

70. Dissing-Olesen, L., Thaysen-Andersen, M., Meldgaard, M., Højrup, P. & Finsen, B. The function of the human interferon-β1a glycan determined in vivo. *J. Pharmacol. Exp. Ther.* **326**, 338–347 (2008).

71. Gervais, D. Protein deamidation in biopharmaceutical manufacture: understanding, control and impact. *J. Chem. Technol. Biotechnol.* **91**, 569–575 (2016).

72. De Weerd, N. A. *et al.* Structural basis of a unique interferon-β signaling axis mediated via the receptor IFNAR1. *Nat. Immunol.* **14**, 901–907 (2013).

73. Deshpande, A., Putcha, B.-D. K., Kuruganti, S. & Walter, M. R. Kinetic analysis of cytokine-mediated receptor assembly using engineered FC heterodimers. *Protein Sci.* **22**, 1100–1108 (2013).

74. Kaltashov, I. A., Bobst, C. E., Abzalimov, R. R., Berkowitz, S. A. & Houde, D. Conformation and Dynamics of Biopharmaceuticals: Transition of Mass Spectrometry-Based Tools from Academe to Industry. *J. Am. Soc. Mass Spectrom.* **21**, 323–337 (2010).

75. Karpusas, M., Whitty, A., Runkel, L. & Hochman, P. The structure of human interferon-β: Implications for activity. *Cellular and Molecular Life Sciences* vol. 54 1203–1216 (1998).

76. Runkel, L. *et al.* Structural and functional differences between glycosylated and non-glycosylated forms of human interferon-β (IFN-β). *Pharm. Res.* **15**, 641–649 (1998).

77. Smith, D. R. *et al.* Inhibition of interleukin 8 attenuates angiogenesis in bronchogenic carcinoma. *J. Exp. Med.* **179**, 1409–1415 (1994).

78. Zhu, Y. M., Webster, S. J., Flower, D. & Woll, P. J. Interleukin-8/CXCL8 is a

growth factor for human lung cancer cells. *Br. J. Cancer* **91**, 1970–1976 (2004).

79. Yuan, A. *et al.* Interleukin-8 messenger ribonucleic acid expression correlates with tumor progression, tumor angiogenesis, patient survival, and timing of relapse in non-small-cell lung cancer. *Am. J. Respir. Crit. Care Med.* **162**, 1957–1963 (2000).

80. Chen, J. J. *et al. Up-Regulation of Tumor Interleukin-8 Expression by Infiltrating Macrophages: Its Correlation with Tumor Angiogenesis and Patient Survival in Non-Small Cell Lung Cancer 1*. (2003).

81. McDonald, S. *et al.* Combined betaseron R (recombinant human interferon beta) and radiation for inoperable non-small cell lung cancer. *Int. J. Radiat. Oncol. Biol. Phys.* **27**, 613–619 (1993).

Merck Serono S.p.A, Rome, Italy; an affiliate of Merck KGaA, Darmstadt, Germany.